Accepted Manuscript

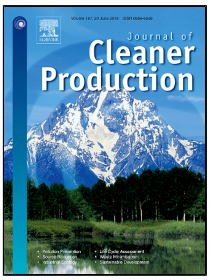

Effects of nanoparticle-enhanced phase change material (NPCM) on solar still productivity

D. Dsilva Winfred Rufuss, L. Suganthi, S. Iniyan, P.A. Davies

PII:	S0959-6526(18)31237-X
DOI:	10.1016/j.jclepro.2018.04.201
Reference:	JCLP 12782
To appear in:	*Journal of Cleaner Production*
Received Date:	19 October 2017
Revised Date:	19 April 2018
Accepted Date:	22 April 2018

Please cite this article as: D. Dsilva Winfred Rufuss, L. Suganthi, S. Iniyan, P.A. Davies, Effects of nanoparticle-enhanced phase change material (NPCM) on solar still productivity, *Journal of Cleaner Production* (2018), doi: 10.1016/j.jclepro.2018.04.201

Effects of nanoparticle-enhanced phase change material (NPCM) on solar still productivity

Dsilva Winfred Rufuss D[a], L. Suganthi[b], S. Iniyan[a], P. A. Davies[c, *]

[a] Institute for Energy Studies, Anna University, Chennai-600025, India

[b] Department of Management Studies, College of Engineering Guindy, Anna University, Chennai-600025, India

[c] Sustainable Environment Research Group, School of Engineering and Applied Science, Aston University, Birmingham, UK, B4 7ET

[*] Corresponding author: p.a.davies@aston.ac.uk

Abstract

This paper investigates the effects of nanoparticle-enhanced phase change material (NPCM) on solar still operation and performance. Technical and economic aspects were considered, to show an advance on earlier works using virgin phase-change materials (PCM). Three types of nanoparticle (TiO_2, CuO and GO) were impregnated individually at 0.3 weight% in paraffin to form NPCM-1, NPCM-2 and NPCM-3 respectively. Experiments were conducted with four solar stills (SS) each of 0.5 m^2 area using respectively paraffin (SSPCM), paraffin-TiO_2 (SSNPCM-1), paraffin-CuO (SSNPCM-2) and paraffin-GO (SSNPCM-3). There was observed an increase in thermal conductivity and a reduction in melting and solidification temperatures, with NPCM compared to PCM. The effects of NPCM on water temperature, storage temperature, hourly and annual productivity were determined. SSPCM, SSNPCM-1, SSNPCM-2 and SSNPCM-3 yielded 3.92, 4.94, 5.28 and 3.66 l/m^2/day respectively, corresponding to 26 and 35% increases in productivity of SSNPCM-1 and 2 respectively over SSPCM. Economic analysis showed cost per liter (CPL) of water of \$0.035, \$0.028, \$0.026 and \$0.13 for SSPCM, SSNPCM-1, 2 and 3 respectively. Considering the advantages in productivity and CPL, SSNPCM-2 can be recommended as the best solar still compared to SSPCM, SSNPCM-1 and 3, providing clean water at less than half the cost of bottled water in India.

Keywords: desalination; phase change material; nanoparticles; paraffin; productivity; techno-economic analysis

Nomenclature

$\overline{X}$	average of experimental observation in each set
AC	annual cost ($)
AMC	annual maintenance cost ($)
ASV	average salvage value
B	latent heat capacity of phase change material (J/kg)
CAS	chemical abstracts service number
C_p	specific heat (J/kg.K)
CPL	cost per liter ($)
CRF	capital recovery factor
D	thermal diffusivity of the sample (m^2/s)
DSC	differential scanning calorimetry
FAC	fixed annual cost ($)
GO	graphene oxide
H	difference in the weights of sample and empty pan (g)
h	difference in the weights of reference and empty pan (g)
JCPDS	joint committee on powder diffraction standards
K	thermal conductivity (W/mK)
k	coefficients of the corresponding phase in TiO_2 nanoparticles
L	latent heat (J/kg)
LFA	laser flash analyzer
M	mass (kg)
N	total number of experimental observations
n	number of sunny days
NPCM	nanoparticle-enhanced phase change material
NPCM-1	titanium dioxide impregnated in paraffin
NPCM-2	copper oxide impregnated in paraffin

NPCM-3	graphene oxide impregnated in paraffin
P	present capital cost ($)
PCM	phase change material
Q	time required for the 50% increase in temperature (s)
R	thickness of the sample (m)
RK	Runga-Kutta method
S	salvage value
SDBS	sodium dodeecycl-benzene surfonate
SFF	sinking fund factor
SHM	sensible heat storage materials
SSNPCM-1	solar still with titanium dioxide impregnated in paraffin as phase change material
SSNPCM-2	solar still with copper oxide impregnated in paraffin as phase change material
SSNPCM-3	solar still with graphene oxide impregnated in paraffin as phase change material
SSPCM	solar still with paraffin as phase change material
T	temperature (°C)
TG/DTA	thermogravimetric/differential thermal analyzer
U	uncertainty (%)
V	voltage of the thermocouple (V)
W	weight fraction (%)
X	average of averages of experimental observation in each set ($l/m^2/day$)
XRD	x-ray diffraction
y	number of years
Z	integrated intensities (a.u)
ρ	density of the sample (kg/m^3)
σ	standard deviation
Subscripts	

Symbols	
A	anatase phase
B	brookite phase
cou	thermocouple
R	rutile phase
r	reference
s	sample

1. Introduction

The solar still is a traditional method for desalinating water using solar energy. Though a simple and reliable device, its productivity is low (usually below 10 l/m^2/day). Therefore much research work has focused on overcoming this limitation (Abujazar et al., 2017; Arunkumar et al., 2016; Dsilva Winfred Rufuss et al., 2018a, 2018b; Kabeel et al., 2018; Rajaseenivasan et al., 2016; Samuel et al., 2016). Storing energy during hours of high solar intensity and releasing it during the nocturnal hours is one of the mechanisms used to improve productivity. In this article, we study the use of cutting-edge heat storage materials to enhance the performance of solar stills in producing clean water.

Insert Table 1(a). Overview of solar stills with sensible heat storage techniques (showing increase in yield where data are provided)

Insert Table 1(b). Overview of solar stills with latent heat storage techniques (showing increase in yield where data are provided)

Energy storage materials vary depending upon the mechanism of heat storage i.e. sensible vs. latent. Table 1 gives an overview of some of the recent research studies using each mechanism. From Table 1(a), it is evident that the addition of sensible heat storage material in the still improves productivity by up to 36% (Kalidasa Murugavel and Srithar, 2011; Manivel et al., 2014; Murugavel et al., 2010; Sakthivel et al., 2010; Shanmugan et al., 2012; Velmurugan et al., 2009, 2008a, 2008b). Latent energy storage is, however, superior to sensible heat energy storage (see Table 1(b)) because of its higher energy storage capacity, resulting in twice the productivity of the unmodified solar still. This is achieved by means

of a phase change material (PCM), placed beneath the solar still, to absorb the thermal energy from water during the charging process and releases it back to the water during discharge. Heat will be stored as latent heat when the temperature of the PCM is in the melting point range, and as sensible heat when outside this range.

Various researchers have used different latent heat energy storage (LHES) materials for solar still applications (Al-harahsheh et al., 2018a; A E Kabeel et al., 2017; Kabeel and El-maghlany, 2018; Manokar et al., 2018). Stearic acid, used underneath the basin, improved the daily productivity by 80% (El-Sebaii et al., 2009). Al-hamadani et al. (2014) compared myristic and lauric acid and found that the former gave better performance. A solar still with lauric acid gave 22% higher productivity over the still with myristic acid. Swetha and Venugopal (2011) also used lauric acid and reported a 36% increase in productivity over that of the conventional still.

Paraffin in particular has been a popular choice of PCM for solar still use. For example, Shalaby et al. (2016) used paraffin to improve the distillate yield by 12%. These authors also carried out an economic analysis of solar stills and found that the cost per liter (CPL) without PCM and with PCM was $0.071 and $0.083 respectively (US dollars) in Egypt. Kabeel and Abdelgaied (2016) used paraffin to obtain a larger increase of 67.2% in productivity. This larger increase may have been due to: (i) the different types of modifications to the absorber [i.e. Shalaby et al. (2016) used a v-corrugated absorber whereas Kabeel and Abdelgaied (2016) used just a flat absorber in solar still]; or (ii) differences in the physical properties (namely melting point, solidification point, thermal conductivity and latent heat) of the paraffin, associated with variations in its chemical composition. The economic analysis of Kabeel and Abdelgaied (2016) concluded that the solar still with paraffin is economically viable, with the CPL being $0.030 for the still with paraffin and $0.032 for the conventional still – less than half the figures reported by Asbik et al. (2016). Ansari et al. (2013) used paraffin PCM in the solar still and achieved productivity of about 4.5 l/m^2/day (also in Morocco) representing a 40.6% increase in the productivity compared to a conventional still. Dashtban and Tabrizi (2011) also used paraffin in a solar still to achieve productivity of about 6.7 l/m^2/day under the climate conditions of Iran. Kabeel et al. (2016) combined hot air injection and addition of paraffin

PCM in Egypt and obtained a productivity of about 9.36 l/m^2/day – a 109% increment in productivity over that of a conventional still. Mousa and Gujarathi, (2016) used paraffin as a latent heat energy storage material in a solar still application to achieve a 49% increase in productivity.

Even though LHES materials give a high storage density, their application is hindered by low thermal conductivity and low heat release. To overcome this, nanoparticles may be introduced to enhance their thermal properties (Dsilva Winfred Rufuss et al., 2017b, 2015; Khodadadi and Hosseinizadeh, 2007; Sari and Karaipekli, 2007; Yang et al., 2014). Nanoparticles increase the thermal conductivity and decrease the melting and solidification temperatures compared to virgin PCM. The improvement in thermal conductivity helps in reducing the charging time of the PCM during the melting period; while the improvement in heat release rate accelerates solidification.

Some researchers have already used nanoparticle-enhanced phase change material (NPCM) in electronic, energy and storage applications. Fang et al. (2009) used nanoparticles encapsulated in tetra-decane as NPCM in an energy storage application, and found that the addition of sodium chloride improved the thermal stability and increased the heat of fusion. Tang et al. (2016) used alumina and graphite as nanoparticles in myristic acid PCM, and found that the thermal conductivity of this NPCM increased by 12% compared to that of unblended PCM. A PCM (paraffin) with copper oxide as NPCM was used by Sciacovelli et al. (2013). They found that the melting time of NPCM was reduced by 15% compared to virgin PCM. Paraffin with graphite was used by Biswas et al. (2014) who concluded that this NPCM had good energy saving potential as compared to virgin PCM. Graphene oxide nano-sheets were used by Yu et al., (2010) and exfoliated graphite was used by Jebasingh (2016) to improve the thermal conductivity of base PCM by 20-60%. Harikrishnan et al. (2013) conducted experiments using stearic acid and titanium dioxide nanoparticles. The results indicated a reduction in melting and solidification time for NPCM compared to PCM. A notable increment of about 70.5% in thermal conductivity was also observed in the NPCM. Motahar et al. (2014) used n-octadecane titanium dioxide as NPCM and found that there was an increase in melting temperature, thermal conductivity and latent heat.

Though nanoparticles have been used by various researchers to modify thermal properties like thermal conductivity, latent heat, melting and solidification temperature of different PCMs in various applications, only very few studies have been done on the use of nanoparticles in solar stills. For example, Mahian et al. (2017) improved the evaporation rate by incorporating a nanoparticle-impregnated heat exchanger, but not using any NPCM. The research gap in this area was highlighted in an extensive review about solar stills and advances in materials for solar stills (Dsilva Winfred Rufuss et al., 2016). To address this gap, we present here a study analysing the viability of nano-PCM (NPCM) in solar still applications, including new experimental studies of NPCM properties and of the performance of solar stills (SS) enhanced by the NPCM (SSNPCM).

Productivity is the key performance parameter of the solar still; however, the productivity when incorporating LHES materials depends on a number of properties such as reliability, stability, thermal conductivity, latent heat, melting and solidifying characteristics of the material. For proper understanding, it is therefore important to analyse first the effects of nanoparticles on PCM properties, and then the effect of the NPCM on the solar still performance in comparison to both conventional solar stills (without PCM) and ones modified with standard PCM. The temperature of PCM material during melting and solidification directly governs the temperature of water (Dashtban and Tabrizi, 2011), improving or impairing the evaporation rate, which in turn influences hourly productivity. Hence the melting and solidification characteristics of PCM and NPCMs also need investigation. In summary, as depicted in Fig.1, there are several input parameters affecting the output of the solar still with PCM as confirmed by earlier modelling studies (Dashtban and Tabrizi, 2011; Tabrizi et al., 2010).

Insert Fig. 1. Block diagram depicting the input, operating and output parameters of solar still with LHES

The objectives of this paper are, therefore to: (i) investigate the thermal properties (thermal conductivity, latent heat, specific heat, melting and solidifying characteristics) of NPCM compared to unblended PCM; and (ii) measure the effect on productivity of including the NPCM in solar stills. This paper presents an experimental investigation together with technical and economic analyses of the results.

2. Materials and methods

This section covers the materials used for NPCM, including their selection, preparation and characterization. It also covers the methods of fabricating and testing the solar stills using the NPCMs.

2.1. Materials

Paraffin and acetamide were earlier found to be the best PCM for application in solar stills (Dsilva Winfred Rufuss et al., 2016; Sharma et al., 2002). Due to the ready availability and chemically inert nature of paraffin as compared to acetamide, paraffin was selected in preference and purchased from Merck Millipore, India (CAS number: 8002-74-2). Titanium dioxide (TiO_2) and copper oxide (CuO) nanoparticles were purchased from Lobha Chemie Private Ltd, India and graphene oxide (GO) nanoparticles from SRL, India, with specified purities of 90, 99 and 98% respectively. Sodium dodeecycl-benzene surfonate (SDBS) was purchased from Sigma-Aldrich, USA and used as capping agent/surfactant during the preparation of NPCM to achieve homogeneous dispersion. For the testing of the solar stills, tap water with total dissolved solids (TDS) of about 1136 ppm was used as the feed water.

2.2. Preparation of NPCM

Based on the recommendations from Lotfizadehkordi et al. (2013) and R. K. Sharma et al. (2016) regarding the preparation of nanocomposites, samples (0.5 kg) of paraffin (base material) were heated to $10^{o}C$ above the melting point by an electronic heater, and then an anionic surfactant, SDBS (sodium dodeecycl-benzene surfonate) was added to the PCM (base material) with the mass ratio of SDBS to nanoparticle of 1:1. The purpose of the surfactant was to ensure stability and homogenous dispersion of the nanoparticles. Then, 0.3 weight% of nanoparticles (TiO_2, CuO or GO) were added to the paraffin to form NPCM-1, NPCM-2 and NPCM-3 nanocomposites respectively. The 0.3% mass fraction was chosen based on earlier studies (Dsilva Winfred Rufuss et al., 2017b; Harikrishnan et al., 2013; Harikrishnan and Kalaiselvam, 2013; Khoshvaght-aliabadi et al., 2014; Lokesh.S et al., 2015; Wang et al., 2012). The choice was based also on the observation that latent heat decreases with mass fraction, suggesting that too high fraction should be avoided (Jegadheeswaran and Pohekar, 2009). The mixtures were then sonicated for 45 min at 40

kHz following Dsilva Winfred Rufuss et al. (2017b), Harikrishnan et al. (2013) and Harikrishnan and Kalaiselvam (2013), noting that longer residing time may result in defects in the lattice structure of NPCM (Dsilva Winfred Rufuss et al., 2017b). Throughout the process, the vibrator temperature was maintained at around 10°C above the melting temperature of PCM to keep the PCM in liquid state. Thus aggregation and settling of nanoparticles in the PCM was avoided.

2.3. Characterization of nanoparticles and NPCMs

The surface morphologies and size of the nanoparticles (TiO_2, CuO and GO) were measured using a Carl Zeiss MA15/EVO18 scanning electron microscope (SEM) and CM-120-Philip transmission electron microscope (TEM). The magnification of the instruments was 50K – 100K. The surface morphologies of the nanoparticles impregnated individually into the PCM are depicted by the SEM images of Fig. 2. The SEM images were analysed using the point-to-point measuring tool (Kundu et al., 2017; M. Sharma et al., 2016) in SmartSEM:EVO 18 version 5.05, Carl Zeiss software to find the average size distribution of nanoparticles with around 15 measurements for each type giving: for TiO_2, average size of 160 nm with range 120-246 nm; and for CuO average of 190 nm with range 150-226 nm. Graphene oxide was in the form of sheets/flakes ranging in size from 418-506 nm. The TEM images (Fig.3) showed a homogenous dispersion of nanoparticles in PCM, and it was found that the paraffin with TiO_2 has spherical shape, paraffin with CuO has cylindrical shape and paraffin with GO has folded foil shape.

Insert Fig. 2. SEM images showing the surface morphology of TiO_2, CuO and GO nanoparticles

Insert Fig. 3. TEM images showing the TiO_2, CuO and GO nanoparticles at high resolution

A Shimatzu diffractometer X-ray, XRD 6000, Japan, was used to study the crystal structure and phase composition of the nanoparticles. The XRD analysis was performed with powders of nanoparticles, with the scattering angle (2θ) between 20° to 80° and the diffraction patterns of the nanoparticles are depicted in Fig. 4. The diffraction peak (2θ) between 55-63 [(hlk) planes: (241), (160)] indicates the brookite phase of TiO_2 nanoparticle (JCPDS

file no: 29-1360) (Harikrishnan et al., 2013; Jebasingh, 2016; Motahar et al., 2014), the peak range 25-49 [(hkl) planes: (101), (004), (200)] confirms the anatase phase (JCPDS file no: 21-1272) and the peak 74.4 [(hkl) planes: (320)] confirms the presence of rutile phase (JCPDS file no: 21-1276) in the TiO_2 sample. The phase composition of the mixed phases (rutile phase, anatase phase, and brookite phase) in TiO_2 nanoparticles was calculated using the following formulae reported by Boppella et al., (2012), and by Zhang and Banfield (2000).

$$W_A = \frac{k_A Z_A}{k_A Z_A + Z_R + k_B K_B} \quad (1)$$

$$W_R = \frac{Z_R}{k_A Z_A + Z_R + k_B K_B} \quad (2)$$

$$W_B = \frac{k_B Z_B}{k_A Z_A + Z_R + k_B K_B} \quad (3)$$

where k_A and k_B are the coefficients of anatase and brookite phase equal to 0.886 and 2.721 respectively (Boppella et al., 2012; Zhang and Banfield, 2000). Z_A, Z_R and Z_B are the integrated intensities; and W_A, W_R and W_B are the weight compositions of anatase, rutile and brookite phases respectively. The percentage volumes of anatase, brookite and rutile phase of TiO_2 nanoparticles were estimated to be 71.6, 23.78and 4.6% respectively. Hence it is confirmed that the characterized TiO_2 nanoparticles have ~71:23:4 mix of anatase (JCPDS file no. 21−1272), brookite (JCPDS file no. 29-1360) and rutile (JCPDS file no. 21-1272) phase respectively. The diffraction peak (2θ) range from 30-70 [(hkl) planes: (111), (200), (202), (113), (220)] confirms the presence of CuO nanoparticles (which is indexed in JCPDS file no: 45-0937) in the corresponding sample (Harikrishnan and Kalaiselvam, 2012). The diffraction peak (2θ) was noted at 9.7 [(hkl) plane: (002)] and 42.59 [(hkl) plane: 100)] confirms the presence of GO (JCPDS file no: 41-1487) in the corresponding sample (Balaji.S et al., 2017; Dsilva Winfred Rufuss et al., 2017b; Sadhasivam and Rigana, 2018).

The XRD showed that TiO_2 and CuO were crystalline whereas GO was amorphous. Many studies have also shown that GO is amorphous (Bhaumik et al., 2017; Kumar, 2015;

Mkhoyan et al., 2009; Shi et al., 2012) and semi-amorphous in nature (Malik et al., 2010; Pei and Cheng, 2011). This amorphous nature of GO is due to the warp from sp^3 C-O (Mkhoyan et al., 2009; Viet et al., 2010). The literature suggests that the amorphous state can be converted to crystalline by annealing graphene oxide at >1000°C, but this transforms GO to graphene (Pei and Cheng, 2011; Renteria et al., 2015; Sheng et al., 2011; Zhao et al., 2012). The XRD results of GO obtained here are consistent with those of other researchers (Shi et al., 2012; Sohail et al., 2017). It is therefore concluded that the amorphous nature of GO is as expected and not defective or detrimental to the thermal properties of NPCM in low temperature energy storage applications such as solar stills (Balaji.S et al., 2017; Dsilva Winfred Rufuss et al., 2017b; Jebasingh, 2016; Mehrali et al., 2013; Shi et al., 2012; Yu et al., 2010).

Once the characterization of nanocomposites was complete, the thermal stability of the composites was tested to find the degradation temperature range and peak degradation point using thermogravimetric analysis. This was done using PerkinElmer, Diamond TG/DTA with operating temperature range of about 40-900°C at a heating rate of about 20°C/min, using nitrogen purge.

Insert Fig. 4. Diffraction patterns confirming the presence of titanium dioxide, copper oxide and graphene oxide nanoparticles

The thermal reliability of the samples were tested using a thermal cycler (BIOER TC-25/H) with cooling and heating rates of 2 and 3°C/s respectively. Thermal conductivity was measured using a laser flash analyzer (LFA 467 HyperFlash-Light Apparatus) at 25°C (room temperature) and with maximum heating rate of 50°C/min. The thermal diffusivity and conductivity ranges of the laser flash analyzer were 0.01–2000 mm^2/s and 0.1–4000 W/m ^{O}C respectively. The pulse width and pulse energy of the xenon flash lamp was up to 20–1200 μs and 10 J/pulse respectively. The vacuum was maintained at <150 mbar. A 2 MHz data acquisition system was used in temperature detection and pulse mapping. The accuracy of specific heat capacity measurement was ±5% and liquid nitrogen was used to cool the furnace. The following equations was used to determine thermal conductivity K (Linseis, 1957):

$$K = D.\,C_p.\,\rho \qquad (4)$$

$$D = \frac{0.1388R^2}{Q} \qquad (5)$$

where D, C_p, ρ and R are respectively the thermal diffusivity, specific heat, density and thickness of the sample and Q is the time required for a 50% increase in temperature. The other thermal properties such as latent heat, specific heat, melting and solidification temperatures were measured using differential scanning calorimetry (Perkin Elmer-DSC 4000). The specific heat of the samples was calculated using the ratio method in DSC analysis (O'Neill, 1966) as follows:

$$C_{ps} = \frac{H}{h}.\frac{M_r}{M_s}.C_{pr} \qquad (6)$$

where H and h correspond respectively to the difference in the weights of sample and empty pan and difference in the weights of reference and empty pan, M_r and M_s are the mass of reference and sample and C_{ps} and C_{pr} correspond to the weight of the sample and reference respectively. The latent heat of the samples was calculated by numerically integrating the peaks of the DSC results (Harikrishnan et al., 2013; Harikrishnan and Kalaiselvam, 2012). The latent heat L was calculated using the following equation (Al-kayiem and Lin, 2014; Sharma et al., 2017)

$$L = mB \qquad (7)$$

where m and B are respectively the mass and latent heat capacity (J/kg) of the PCM. The instrument specifications and accuracies are tabulated in Table 2. Further details of these measurements were already described in our previous work (Dsilva Winfred Rufuss et al., (2017b).

2.4. Fabrication and test of solar still

Four solar stills each of 0.5 m^2 area were fabricated from aluminium-6061 sheet (Fig. 5 and Fig. 6): (i) with PCM (SSPCM); (ii) with NPCM-1 (SSNPCM-1); (iii) with NPCM-2 (SSNPCM-2) and (iv) with NPCM-3 (SSNPCM-3). The base of each still was coated with asphalt black paint to improve the absorptivity of solar radiation onto the basin. There was

a reservoir of 2 cm height below the basin which held 10 liters of the NPCM. From the literature, it was inferred that the volume of saline feed water must be less than that of the volume of PCM (El-Sebaii et al., 2009; A. E. Kabeel et al., 2017; Kabeel and El-Agouz, 2011; Somanchi et al., 2015), and hence 9 liters of saline water was fed into the still. A transparent glass cover with 2.5 mm thickness was used as a cover inclined at 13° to the horizontal. The bottom and sides of the system were insulated using polystyrene foam to minimize the heat loss to the surroundings (Fig. 5). K-type thermocouples measuring the temperatures of the water, glass, enclosed air, and PCM storage units were fitted in each of the four solar stills. The thermocouples were calibrated at the Instrumentation and Calibration Laboratory, Anna University, Chennai-600025 using a rational polynomial functional approximation (Clifford, 2016):

$$T_{cou} = T_o + \frac{(V - V_o)\left[p_1 + (V - V_o)\left(p_2 + (V - V_o)(p_3 + p_4(V - V_o))\right)\right]}{1 + (V - V_o)\left[q_1 + (V - V_o)\left(q_2 + q_3(V - V_o)\right)\right]} \quad (8)$$

where T and V are the temperature and voltage of the thermocouple. T_o, p_1, p_2, p_3, V_o, q_1, q_2 and q_3 are coefficients calculated by carrying out a least square curve fit to the National Institute of Standards and Technology (NIST) data base, giving respective values (over a temperature range -100 to +100 ^{o}C) of -8.79, -0.344, 25.67, -0.498, -0.447, -0.0448, 0.000238, -0.02039 and -0.00184 (NIST ITS-90 Thermocouple Database, 1993).

Outdoor experiments were performed at the Institute for Energy Studies, Department of Mechanical Engineering, Anna University, Chennai (latitude 13.08^{O} N, longitude 80.27^{O} E), India, during the months of April and May 2016 ensuring the weather was stable over the period of observation. Temperatures were observed from 8.00 to 20.00 hrs at hourly intervals. The period of the experiments was 10 days (4th, 6th, 12th, 14th & 22nd April; and 2nd, 5th, 19th 18th & 25th May) allowing each hourly measurement to be averaged over 10 readings. An anemometer and solarimeter were used to measure the wind velocity and solar radiation respectively. The radiation attributes only a minimal effect in the accuracy of the thermocouple, especially K- and R-type thermocouples (J.C. Jones, 1995; Shannon and Butler, 2003), thus not affecting the results significantly. The accuracy, range and error of all instruments is summarised in Table 2.

Insert Fig. 5. Schematic diagram of SSPCM, SSNPCM-1, SSNPCM-2 and SSNPCM-3

Insert Fig. 6. Pictorial view of SSPCM, SSNPCM-1, SSNPCM-2 and SSNPCM-3

Insert Table 2. Accuracy and range of the various measuring instruments used

3. Uncertainty analysis

An error analysis was performed to check the impact of errors in the experimental observations on the techno-economic analysis and conclusions. The uncertainty of measurements (Table 3) was calculated based on the formulae given below, as proposed by Sandeep et al., (2015), Alaudeen et al., (2014), Kumar and Tiwari, (1996) and Velmurugan et al., (2008a), in which U_i corresponds to internal uncertainty, $\overline{X}$ corresponds to the average of experimental observations of productivity in each set, X_i corresponds to the average of averages of experimental observations in each set, N is the total number of experimental observations and N_o is the number of observation in each set.

$$\text{Uncertainity percentage} = \frac{U_i}{X_i} \text{ x } 100 \quad (9)$$

$$U_i = \frac{\sqrt{\sigma_1{}^2 + \sigma_2{}^2 + \sigma_3{}^2 + \ldots + \sigma_N{}^2}}{N} \quad (10)$$

$$\sigma = \frac{\sqrt{\sum (X - \overline{X})^2}}{N_o} \quad (11)$$

Using the above, the values of U_i, X_i and percentage uncertainty associated with the experimental observations of the productivity of solar stills was calculated (see Table 3). The values of U_i for SSPCM, SSNPCM-1, SSNPCM-2 and SSNPCM-3 were found to be 0.0031, 0.00275, 0.0026 and 0.00218 and their corresponding X_i values was 0.1507, 0.1860, 0.2030 and 0.1407 respectively. The uncertainty percentage associated with the experimental productivity of SSPCM, SSNPCM-1, SSNPCM-2 and SSNPCM-3 was found to be 2.06, 1.47, 1.28 and 1.54% respectively. The uncertainty in this experiment is in line with that achieved by the other researches such as Tiwari et al., (1998) with 1.5%, Omara et al., (2015) with 2.2%, Manokar et al., (2018) with 3.04%, Kumar and Tiwari (1996) with

5% and Eltawil and Omara (2014) with 2.3% - thus confirming that the errors are sufficiently small and they will not impact on the conclusions of the study. Further, the errors in productivity only cause a variation in the 3rd and 4th decimal places of the corresponding cost per liter (CPL, section 5) which as such is negligible.

Insert Table 3. Percentage uncertainties showing the values of U_i and X_i

4. Results and discussion

In this section, the results relating to the properties of NPCM, and to the performance of the solar stills incorporating them, are presented and discussed from the technical perspective.

4.1. Effect of nanoparticles on thermal reliability and stability of PCM

Resulting from the tests of thermal reliability and stability (section 2.3), Fig 7 shows the phase change temperature against the number of cycles during charging and discharging. The shift in melting temperature was found to be -1.55, -1.69, -1.71, -2.07% and in solidification temperature -1.86, -1.81, -2.18, -0.17% for PCM, NPCM-1, 2 and 3 respectively; as such sufficiently small not to cause any deleterious effect on performance.

Though there is a slight deviation in melting and solidification point in Fig. 7, from the melting and solidification peaks obtained from the DSC results (see Fig. 10), this finding is consistent with observations by other researchers (Harikrishnan et al., 2013; Harikrishnan and Kalaiselvam, 2013; Silakhori et al., 2013). The phase transition of an energy storage material typically begins ± 1 to 3°C before/after the melting and solidification peaks (points) obtained by DSC (Harikrishnan et al., 2013; Harikrishnan and Kalaiselvam, 2012; Henisch et al., 1973; Parameshwaran et al., 2012; Silakhori et al., 2013; Suchitra, 2004).

The thermogravimetric curves of PCM, NPCM-1, NPCM-2 and NPCM-3 showed degradation of the base material (paraffin) over the range 130-180°C (Fig. 8). Nanoparticles caused the degradation temperature range to increase to 150-280°C, 160-300°C and 165-298°C for NPCM-1, NPCM-2 and NPCM-3 respectively; and the corresponding percentage increases in the stability of the composites were 15.4, 23.1 and 26.9% respectively compared to the base material. The reason for the increase in stability may be the bond breakage of polymers to monomers. The peak degradation temperatures for PCM, NPCM-1, NPCM-2 and NPCM-3 were found to be 232°C, 250°C, 272°C and 268°C respectively. Hence it is

evident that nanoparticles with paraffin (NPCM-1, 2 and 3) showed improved thermal stability over virgin paraffin.

Insert Fig. 7. Phase change temperature variation against thermal cycle during charging and discharging

Insert Fig. 8. TGA curves of PCM, NPCM-1, NPCM-2 and NPCM-3 showing improved stability

4.2. Effect of nanoparticles on thermal conductivity, specific and latent heat of PCM

The results of the thermal conductivity measurements (Fig. 9) gave 0.325, 0.335 and 0.523 W/mK for NPCM-1, NPCM-2 and NPCM-3, showing enhancements of 25.0, 28.8 and 101.2% respectively over of pure PCM (0.26 W/mK). With regard to specific heat capacity, the results were: 2.94, 2.85 and 2.87 J/gK (NPCM1, 2 and 3 respectively) indicating 3.06, 2.3 and 1.3% decreases relative to pure PCM (2.90 J/gK). As expected, the lower specific heat capacity of the nano-material used for the impregnation, results in a lowering of the specific heat of the final nano-composite and vice-versa (He et al., 2012). The latent heat of the samples are calculated by numerical integration of melting and solidification peak achieved from the DSC measurements (Fig. 10).

There was an interesting trend in the latent heats of the NPCMs follows. The latent heats of PCM, NPCM-1, NPCM-2 and NPCM-3 were measured as 102, 118, 168 and 64.7 kJ/kg respectively; therefore, NPCM-1 and NPCM-2 showed a 15.7 and 64.7% increase respectively; while NPCM-3 showed a 39.7% decrease.

The increase may be attributed to mechanisms such as the surface charge states of nanoparticles, layering in the liquid-solid phase, and movement of phonons (He et al., 2012; Lee et al., 2006). Whereas the decrease in latent heat may be due to carbon and oxygen bond arrangement in lattice, sp^2 hybridization, dispersing property with organic solvents, hydrophilic material, molecular sieves, volume variation during expansion and organic covalent functionalization of GO (Dsilva Winfred Rufuss et al., 2017b; He et al., 2012; Lee et al., 2006). However, the improvement or impairment depends on the type of nanoparticle and base material.

Insert Fig. 9. NPCM-1, NPCM-2 and NPCM-3 showing improved thermal conductivity compared to PCM

Insert Fig. 10. DSC curves showing melting and solidification characteristics of PCM, NPCM-1, NPCM-2 and NPCM-3

4.3. Effect of nanoparticles on melting and solidification characteristics of PCM

The nanoparticles also changed the melting and solidification characteristics of the impregnated PCM (see Fig. 10). The melting and solidification points of paraffin (PCM) were found to be 63.5 and 59°C respectively. With the impregnation of TiO_2 nanoparticles (NPCM-1) these decreased to 58.5 and 55°C respectively, corresponding to 7.9 and 6.8% decreases. With CuO nanoparticles (NPCM-2), corresponding values were 59 and 55°C i.e. 7.1 and 6.8% decreases respectively. GO showed the highest decrement in melting and lowest decrement in solidification point, resulting in 57.5 and 56°C respectively i.e. decreases of 9.4 and 5.1% against pure PCM. To summarize, compared to PCM, the thermal conductivity of all three NPCMs was higher and the melting and solidification temperatures were lower. The latent heat of NPCM-3 was lower than that of PCM; whereas the latent heat of NPCM-1, NPCM-2 was higher.

4.4. Effect of nanoparticles impregnated PCM on solar still performance

The hourly yields of the four solar stills tested are depicted in Fig. 11. SSNPCM-1 and SSNPCM-2 gave higher yield than SSPCM and SSNPCM-3. This was because, during charging, the thermal conductivity was relatively good for SSNPCM-1 and SSNPCM-2 and during discharging the latent heat of SSNPCM-1 and SSNPCM-2 was much better than SSPCM and SSNPCM-3. Even though the water temperature of SSPCM (see Fig. 14) was higher than in the other stills till 14:00 hrs, the difference in water and glass temperature are almost same for SSPCM, SSNPCM-1 and SSNPCM-2 and hence the hourly productivity of SSPCM, SSNPCM-1 and SSNPCM-2 do not show much variation till 14:00 hrs. However the maximum variation in hourly yield was witnessed during the discharge process.

The cumulative yields of the four stills (SSPCM, SSNPCM-1, SSNPCM-2 and SSNPCM-3) are shown in Fig. 12, together with the results from a conventional still (no PCM) as reported by Sakthivel et al. (2010). This study was chosen for comparison, because it used

a solar still of similar design and tested under similar to conditions, and in the same location, as in the current study. From the graph, it is inferred that SSNPCM-2 shows highest productivity, followed by SSNPCM-1, SSPCM, SSNPCM-3 and then the conventional still. The productivities of conventional still, SSPCM, SSNPCM-1, SSNPCM-2 and SSNPCM-3 were found to be 3.00, 3.92, 4.94, 5.28 and 3.66 l/m^2/day respectively. There was 23, 39.27, 43.18, 18.03% improvement observed in the productivity of SSPCM, SSNPCM-1, SSNPCM-2 and SSNPCM-3 respectively above the productivity of the conventional still. As there are no productivity boosters in the conventional still, it yields lower productivity than the others. When the solar stills with similar configuration (except conventional still) are considered, the percentage increases in the productivity of SSNPCM-1 and SSNPCM-2 as compared to SSPCM were found to be 26.0 and 35% respectively. There was a 6.6% decrease in the productivity observed in SSNPCM-3 relative to that of SSPCM. This deterioration occurred because, even though the thermal conductivity of NPCM-3 was highest among PCM, NPCM-1 and NPCM-2, the latent heat of NPCM-3 was very low, and hence the low heat release to the water during discharge resulted in low productivity.

It should also be noted that, due to the higher thermal conductivity of GO, SSNPCM-3 charged faster than the other stills as confirmed by analysis of the temperature of the water and storage units (see Fig. 14 and Fig. 16). During discharge when the temperature of the storage unit reduces to within the range of the solidification [usually ±3 ^{O}C of solidification point (Ansari et al., 2013; Dashtban and Tabrizi, 2011; Dsilva Winfred Rufuss et al., 2017a)], the storage unit releases heat to the water. Since the latent heat of NPCM-3 (paraffin+GO) is very low as compared to other NPCMs, the amount of heat liberated by the storage unit to the water is also low as compared to the other stills. This in turn reduces the condensate yield of SSNPCM-3 during the solidification process. Thus, SSNPCM-3 yields the least productivity. On the other hand, the latent heat of NPCM-2 is very high (as explained in section 4.2.) as compared to the other NPCMs, which liberates more heat to the water during solidification. As a result SSNPCM-2 had the best yield.

The order of merit in terms of increasing productivity was therefore: SSNPCM-2, SSNPCM-1, SSPCM and SSNPCM-3. To achieve better yield from the solar still with storage (PCM), the PCM must be selected considering thermal conductivity and latent heat.

These two properties will have more impact during melting and solidification period. Maintaining higher temperature difference between water and glass cover is also important to improve the productivity. Thus, SSNPCM-1 and SSNPCM-2 showed better performance than SSPCM.

Insert Fig. 11. Comparison of hourly yield for SSPCM, SSNPCM-1, SSNPCM-2 and SSNPCM-3

Insert Fig. 12. Cumulative daily yield of SSPCM, SSNPCM-1, SSNPCM-2 and SSNPCM-3

The productivities of the present study are compared against previous results from the literature in Table 4. However, the productivity of solar still varies with location, latitude, solar intensity, ambient temperature and wind velocity. Integrating the solar still with Nano-PCM (paraffin+ copper oxide and paraffin+ titanium dioxide) is technically better than with virgin PCM's.

Insert Table 4. Productivity comparison (where data are provided)

The measurements of the various temperatures, including glass temperature, enclosed air temperature, water temperature and storage temperature, were useful to help explain the increase in yield. The impregnation of nanoparticles with PCM affects the water temperature, storage temperature and glass temperature more, which in turn causes increase/decrease in the condensate yield. The effect of NPCM on water temperature and storage temperature are discussed next, in order to provide insights about the enhancements in performance obtained.

The hourly variation of solar radiation and wind velocity are depicted in Fig. 13. Peak intensities of 1176, 1173, 1115, 1076 W/m^2 was achieved at 13:00, 12.00, 11.00 hrs respectively. The water temperature varies according to the thermal conductivity and latent heat of the different materials used (see Fig.14).

Insert Fig. 13. Hourly variation of solar intensity and wind velocity

SSPCM vividly clearly shows higher temperature than SSNPCM-1, SSNPCM-2 and SSNPCM-3 till 14.00 hrs. This was because, the thermal conductivity was comparatively

high for NPCM-1, NPCM-2 and NPCM-3 than for PCM, and hence the rate of melting of NPCM-1, NPCM-2 and NPCM-3 was faster. This effect in turn increased the water temperature of SSPCM and decreased the water temperature of SSNPCM-1, SSNPCM-2 and SSNPCM-3. After 15.00 hrs the order reversed: SSNPCM-2 dominated over SSNPCM-1, SSNPCM-3 and SSPCM. This trend was achieved because the latent heat of PCM, NPCM-1, NPCM-2 and NPCM-3 was released to water. NPCM-2 has higher latent heat than others. To summarize, for a solar still with PCM, water temperature mainly depends on two parameters – thermal conductivity and latent heat. Thermal conductivity is certainly required during the charging period and latent heat is apparently important during the discharge process.

Insert Fig. 14. Comparison of water temperatures of SSPCM, SSNPCM-1, SSNPCM-2 and SSNPCM-3

The variation of absorber plate temperature for SSPCM, SSNPCM-1, 2 and 3 is depicted in Fig. 15 and it is clear from the Fig. 15 that absorber plate temperature of SSPCM dominates the other stills (SSNPCM-1, 2 and 3) till 13:00 hrs. After 15:00 hrs, the absorber plate temperature of SSNPCM-2 surpassed the rest. This is due to the fast solidification rate of NPCM-2 than that of PCM, NPCM-1 and 3. The absorber plate temperature of SSNPCM-1 and 2 was more or less the same; however, a slight improvement in temperature is observed in SSNPCM-2 as compared to SSNPCM-1. In summary, the absorber plate provides direct thermal contact between the PCM and water. The heat is absorbed and transmitted through basin from water to storage material and vice-versa during charging and discharging period.

Insert Fig. 15. Comparison of absorber plate temperatures of SSPCM, SSNPCM-1, SSNPCM-2 and SSNPCM-3

The addition of nanoparticles had interesting effects on the temperature of the PCM storage units (Fig. 16). The storage unit temperature of SSPCM was initially lower than that of the other stills. This was because the melting time was longer for SSPCM than for the stills with nanoparticles. Moreover, during discharge, the storage temperature of SSPCM was relatively high because of the slower solidification. For SSNPCM-3, storage temperature increased then decreased. Till 15.00 hrs, the temperature in SSNPCM-3 was higher than the other storage temperatures; then after 15.00, SSNPCM-3 lagged behind the other stills in

temperature. Among the four stills, SSNPCM-2 showed considerably better performance in storage temperature than the rest. This improvement is attributed to the increase in thermal conductivity (from 0.26 to 0.335 W/mK), and latent heat (from 102 to 168 kJ/kg) and reduction in melting point (from 63.5 to 59°C) and solidification point (from 59 to 55°C) properties.

Insert Fig. 16. Temperatures in storage unit of SSPCM, SSNPCM-1, SSNPCM-2 and SSNPCM-3

In summary, thermal conductivity, melting and solidification points together play a vital role in increasing/decreasing the storage unit temperature during charge and discharge of energy. While the LHES material is charging, the energy is stored in the form of sensible heat till it reaches its melting point. Once the melting point is reached, the phase of the LHES material starts to change from solid to liquid and at that time the energy is stored in the form of latent heat within the LHES material [since sensible heat is very low and often neglected at this time (Sharma et al., 2017)]. Once phase saturation is attained by the LHES material (i.e. after its complete liquid state), again the energy is stored in the form of sensible heat within the LHES material (Al-harahsheh et al., 2018b; Arunkumar et al., 2013). Thermal conductivity and melting point are the predominant properties which vary the rate of melting of LHES material during charging. Latent heat and solidification point are the influencing properties during discharge. During discharge process, the temperature of LHES material gradually decreases. At that time the LHES material releases the heat in the form sensible heat and once the phase transition temperature is reached during solidification process, the phase of LHES material starts changing from liquid to solid. The LHES material releases latent heat when it is in its phase transition temperature range (Al-harahsheh et al., 2018b; Arunkumar et al., 2013). When the temperature decreases further (i.e. below its phase transition temperature range), it releases a feeble amount of heat (i.e. sensible heat) during the rest of the process (Al-harahsheh et al., 2018b; Arunkumar et al., 2013). Thus the temperature of storage unit varies during charging and discharging process for various LHES material.

The temperature difference between the water and glass cover is crucial for achieving better hourly and daily distillate yield. For the various stills considered in this research, the

difference is depicted in Fig. 17. Some researchers found a minimum temperature difference needed to induce evaporation in the still (Sakthivel et al., 2010; Sakthivel and Shanmugasundaram, 2008). There are several studies showing that an increase in temperature difference between water and glass cover in turn increases the amount of distillate yield (Al-hamadani et al., 2014; Ansari et al., 2013; Asbik et al., 2016; Kabeel et al., 2016). The absorptivity coefficient of glass (0.05) is very low as compared to black asphalt paint (0.91) coating the absorber plate, and this temperature difference between water and glass temperature in turn influences the productivity. In this research, SSNPCM-2 and SSNPCM-1 exhibited a higher temperature difference between the water and the glass cover, compared to that of the other stills.

The increase/decrease in temperature difference depends on the atmospheric temperature, enclosed air temperature, wind velocity, cloud shading, etc. The temperature difference between water and glass cover influences the productivity of a solar still (A.KAbu-Hijleh, 1996; Jubran, 2002; Muftah et al., 2014; Prakash and Velmurugan, 2015; Sharshir et al., 2016). In our experiment, at 09:00 hrs the wind velocity was lower than at 08:00 hrs, causing the glass temperature at 9:00 to increase above that at 08:00 hrs, providing a low temperature difference between water and glass cover thus yielding lower productivity at 9:00 than at 8.00 hrs despite the increased solar radiation at 9.00 hrs.

For SSPCM, there was a higher water temperature observed and hence enclosed air temperature will be relatively high, which in turn increases the glass temperature. Similar characteristic was observed for SSNPCM-3 during discharge process. Hence those two stills (SSPCM, SSNPCM-3) have poor output productivity as compared to SSNPCM-1 and SSNPCM-2. The temperature difference between water and glass cover at 12:00 hrs is higher than that of the temperature difference between water and glass cover at 13:00 hrs. Also, the wind velocity at 12:00 hrs is less than that of 13:00 hrs; this reduces the temperature of glass and in turn increases the difference between water and glass cover yielding higher productivity at 12:00 hrs. Therefore the productivity may be maximum at a time before the water reaches its maximum temperature when the temperature difference between water and glass cover is maximum (Arunkumar et al., 2013; Dashtban and Tabrizi, 2011; Kabeel et al., 2012; Samuel et al., 2016; Shalaby et al., 2016). Hence the hourly

productivity is maximum before the water attains its maximum temperature. To summarise, the temperature difference between water and glass cover varies linearly with the productivity.

Insert Fig. 17. Water and glass cover temperature difference in SSPCM, SSNPCM-1, SSNPCM-2 and SSNPCM-3

5. Economic analysis

It is important to analyse the cost of solar stills considering nanoparticles with paraffin as a novel material for energy storage in this application. The cost analysis was carried out using the method proposed by Fath et al., (2003) to arrive at a cost per liter (CPL) in each case. The present capital cost of the solar stills is given in Table 5 (a conversion rate of 67 Indian Rupees per US Dollar is used). The inputs to the calculation were present capital cost (from Table 5) and capital recovery factor (CRF). Number of years of operation (y) and CRF are assumed to be 10 years and 0.177 respectively (El-Bialy et al., 2016; Kabeel et al., 2010). Using the inputs and assumptions, the outputs such as fixed annual cost (FAC), sinking fund factor (SFF), salvage value (S), average salvage value (ASV) and annual maintenance cost (AMC), annual cost (AC), average annual productivity (M) and cost per liter (CPL) associated with the solar stills for Indian climatic condition were arrived using the following expressions and depicted in Table 6.

Insert Table 5. Capital cost of SSPCM, SSNPCM-1, SSNPCM-2 and SSNPCM-3

Insert Table 6. Cost analysis of SSPCM, SSNPCM-1, SSNPCM-2 and SSNPCM-3

$$\mathrm{FAC} = \mathrm{P} * \mathrm{CRF} \quad (12)$$

$$\mathrm{SFF} = \frac{\mathrm{i}}{(\mathrm{i}+1)^{\mathrm{y}-1}} \quad (13)$$

$$\mathrm{S} = 0.2 * \mathrm{P} \quad (14)$$

$$\mathrm{ASV} = \mathrm{SFF} * \mathrm{S} \quad (15)$$

$$\mathrm{AMC} = 0.15 * \mathrm{FAC} \quad (16)$$

$$AC = FAC + AMC - ASV \quad (17)$$

$$M = c * n \quad (18)$$

where 'c' is the distillate yield per day and the values are mentioned in the above section and 'n' is considered to be approximately 250 days

$$CPL = \frac{AC}{M} \quad (19)$$

The total cost required for fabrication of SSPCM, SSNPCM-1, SSNPCM-2 and SSNPCM-3 respectively was \$89.45, \$89.67, \$89.63 and \$309.45 respectively (Table 5). The total cost of SSNPCM-3 was much higher as compared to other stills because of graphene oxide nanoparticles impregnated in SSNPCM-3 which costs around 168 \$/gm (Dsilva Winfred Rufuss et al., 2017b).

The annual maintenance cost for SSPCM, SSNPCM-1, SSNPCM-2 and SSNPCM-3 was found to be \$2.374, \$2.38, \$2.37 and \$8.21 respectively. The percentage increase in the maintenance cost of SSNPCM-1, SSNPCM-2 over that of SSPCM was found to be 0.24% and 0.20% respectively. The graphical representation of annual productivity and CPL for each still is depicted in Fig. 18. The annual productivity of SSPCM, SSNPCM-1, SSNPCM-2, and SSNPCM-3 was calculated by product of the daily yield and number of sunny days (which is considered to be approximately 250). The annual productivity was found to be 490, 617, 660 and 453 liters respectively. SSNPCM-2 gave the highest productivity followed by SSNPCM-1 i.e. a 25.9% and 34.7% increase in productivity noted for SSNPCM-2 and SSNPCM-3 over SSPCM.

The CPL of SSPCM, SSNPCM-1, SSNPCM-2 and SSNPCM-3 was found to be \$0.035, \$0.028, \$0.026 and \$0.133 respectively. Thus SSNPCM-2 gave the cheapest water and SSNPCM-3 the most expensive. Considering both technical and economic aspects, SSNPCM-2 holds the first place with an annual productivity of about 660 liters and \$0.026 cost per liter. SSNPCM-1 and SSPCM hold second and third positions with annual productivities of 617 and 490 liters respectively. The CPL of SSNPCM-1 and SSPCM corresponds to \$0.028 and \$0.035 respectively. SSNPCM-3 holds the last place with the

least annual productivity and high CPL. The comparison of CPL of various solar stills is depicted in Table 7.

Insert Table 7. Comparison of CPL for various solar stills with PCM

For comparison, the cost of bottled water (not the selling price) in India is around $0.06 per liter which includes the cap cost, label cost, treatment cost, carton cost, transportation cost and other miscellaneous cost; however, bottled water is typically being sold at $0.22 per liter (Chandra Bhushan, 2006). The CPL of water from SSPCM, SSNPCM-1 and SSNPCM-2 are 40.8, 53.3 and 56.6% respectively lower than the CPL of the bottled water in India. Only SSPCM-3 shows higher cost than the bottled water cost, by 121.6%. The CPL of water from a simple conventional solar still in India is $0.035 (Ranjan and Kaushik, 2013). There was 20 and 25% respectively decrease observed in the CPL of water from SSNPCM-1 and SSNPCM-2 as against simple conventional solar still. Thus, SSNPCM-1 and SSNPCM-2 can be recommended, whereas SSNPCM-3 is unfit for commercialization.

Hence the solar still with NPCM-1 (paraffin+ titanium dioxide) and NPCM-2 (paraffin+ copper oxide) are technically and economically sound for solar still application and preferred over the solar still with PCM (paraffin). In particular SSNPCM-2 gives the best results compared to SSPCM, SSNPCM-1 and SSNPCM-3.

Insert Fig. 18. Overall comparison of various parameters for SSPCM, SSNPCM-1, SSNPCM-2 and SSNPCM-3

6. Conclusions

The performance of solar stills with nanoparticle-enhanced PCM (NPCM) has been investigated. Four solar stills were fabricated with PCM (paraffin), and NPCM-1, NPCM-2 and NPCM-3 (containing TiO_2, CuO and GO nanoparticles respectively) and experimentally observed in Indian climatic conditions. The error analysis has confirmed that the percentage error associated with the experiments is not significant. The following conclusions have been obtained:

1. The addition of nanoparticles decreases the melting and solidifying temperature of virgin PCM. There was 7.87, 7.08 and 9.44% decrease in melting temperature and 6.77, 6.77 and

5.08% decrease in solidifying temperature observed in NPCM-1, NPCM-2 and NPCM-3 respectively, compared to virgin PCM.

2. The addition of TiO_2, CuO and GO nanoparticles improves the thermal conductivity of base material (paraffin) by 25.0, 28.8 and 101% respectively.

3. Two properties, namely latent heat and thermal conductivity, play a vital role during melting and solidification respectively. High thermal conductivity helps in decreasing the melting time of PCM; while increased latent heat helps in releasing more heat during solidification.

4. The productivity of a solar still (SS) increases with the addition of NPCM. There were 26.0% and 35% increments in productivity for SSNCPM-1 and SSNPCM-2 respectively, compared to SSPCM. Improvements of 23.0, 39.3, 43.2 and 18.0% were obtained for SSPCM, SSNPCM-1, SSNPCM-2 and SSNPCM-3, against the productivity of a conventional still.

5. SSNPCM-2 gave the highest annual productivity of about 1320 liters per m^2. Hence this still is technically viable due to the combined effect of all of its properties: thermal conductivity, latent heat, stability, reliability, melting and solidification temperatures. The technical disadvantage of the other stills may be due to the poorer thermal conductivity, latent heat, stability, melting and solidifying temperatures as compared to SSNPCM-2.

6. The least cost per liter was achieved by SSNPCM-2 at $0.026.

7. Even though NPCM-3 has the highest thermal conductivity, it has low productivity because of its poor latent heat. When considering the economic aspects, SSNPCM-3 shows poor CPL and annual productivity. Hence it is not a potential candidate for solar still applications.

SSNPCM-2 is therefore recommended as a very promising candidate for solar still applications, as it surpasses the other stills, including conventional solar stills, SSPCM, SSPCM-1 and SSPCM-3. SSNPCM-2 had daily productivity, annual productivity and CPL of about 5.28 l/m^2/day, 1320 l/m^2/year and $0.026 respectively. This CPL is less than half the cost of bottled water in India, and a fraction of the typical selling price.

In summary, nanoparticle (copper oxide and titanium dioxide)-enhanced paraffin has better potential as an energy storage material as compared to virgin paraffin, especially in the solar still application, from both technical (higher productivity) and economic (lower CPL) perspectives. For further research, we recommend studying and optimising the fraction of nanoparticle, focussing on CuO; and we also recommend developing comprehensive mathematical models to assist in these optimisations.

Acknowledgements

The authors gratefully acknowledge DST and the British Council for providing financial support under the UKIERI Thematic Partnership (DST/INT/UK/P-86/2014). Also, one of the authors Mr. Dsilva Winfred Rufuss gratefully acknowledges the Maulana Azad National Fellowship (MANF) program by the Ministry of Minority Affairs, University Grants Commission (UGC) New Delhi, Proceeding No. MANF-2015-17-TAM-48968.

References

A.KAbu-Hijleh, B., 1996. Enhanced solar still performance using water film cooling of the glass cover. Desalination 107, 235–244.

Abujazar, M.S.S., Suja, F., Ibrahim, I.A., Kabeel, A.E., Sharil, S., 2017. Productivity modelling of a developed inclined stepped solar still system based on actual performance and using a cascaded forward neural network model. Journal of Cleaner Production. doi:10.1016/j.jclepro.2017.09.092

Al-hamadani, A.A.F., Shukla, S.K., Dwivedi, A., 2014. Experimental Investigation and Thermodynamic Performance Analysis of a Solar Distillation System with PCM Storage: Energy and Exergy. Distributed Generation & Alternative Energy Journal 29, 7–24. doi:10.1080/21563306.2014.11442728

Al-harahsheh, M., Abu-arabi, M., Mousa, H., Alzghoul, Z., 2018a. Solar desalination using solar still enhanced by external solar collector and PCM. Applied Thermal Engineering 128, 1030–1040. doi:10.1016/j.applthermaleng.2017.09.073

Al-harahsheh, M., Abu-Arabi, M., Mousa, H., Alzghoul, Z., 2018b. Solar desalination using solar still enhanced by external solar collector and PCM. Applied Thermal Engineering

128, 1030–1040. doi:10.1016/j.applthermaleng.2017.09.073

Al-kayiem, H.H., Lin, S.C., 2014. Performance evaluation of a solar water heater integrated with a PCM nanocomposite TES at various inclinations. Solar Energy 109, 82–92. doi:10.1016/j.solener.2014.08.021

Alaudeen, A., Johnson, K., Ganasundar, P., Syed Abuthahir, A., Srithar, K., 2014. Study on stepped type basin in a solar still. Journal of King Saud University - Engineering Sciences 26, 176–183. doi:10.1016/j.jksues.2013.05.002

Ansari, O., Asbik, M., Bah, A., Arbaoui, A., Khmou, A., 2013. Desalination of the brackish water using a passive solar still with a heat energy storage system. Desalination 324, 10–20. doi:10.1016/j.desal.2013.05.017

Arunkumar, T., Denkenberger, D., Ahsan, A., Jayaprakash, R., 2013. The augmentation of distillate yield by using concentrator coupled solar still with phase change material. Desalination 314, 189–192. doi:10.1016/j.desal.2013.01.018

Arunkumar, T., Velraj, R., Denkenberger, D.C., Sathyamurthy, R., Kumar, K.V., Ahsan, A., 2016. Productivity enhancements of compound parabolic concentrator tubular solar stills. Renewable Energy 88, 391–400. doi:10.1016/j.renene.2015.11.051

Asbik, M., Ansari, O., Bah, A., Zari, N., Mimet, A., El-Ghetany, H., 2016. Exergy analysis of solar desalination still combined with heat storage system using phase change material (PCM). Desalination 381, 26–37. doi:10.1016/j.desal.2015.11.031

Balaji.S, Rukmanikrishnan, B., Rigana, M.F., Sarojadevi, M., 2017. Influence of Graphene Oxide on Thermal , Electrical , and Morphological Properties of New Achiral Polyimide. POLYMER ENGINEERING AND SCIENCE 1–10. doi:DOI 10.1002/pen.24600

Bhaumik, A., Haque, A., Taufique, M.F.N., Karnati, P., Patel, R., Nath, M., Ghosh, K., 2017. Reduced Graphene Oxide Thin Films with Very Large Charge Carrier Mobility Using Pulsed Laser Deposition. Journal of Material Sciences & Engineering 6, 2169–22. doi:10.4172/2169-0022.1000364

Biswas, K., Lu, J., Soroushian, P., Shrestha, S., 2014. Combined experimental and numerical evaluation of a prototype nano-PCM enhanced wallboard. Applied Energy 131, 517–529.

doi:10.1016/j.apenergy.2014.02.047

Boppella, R., Basak, P., Manorama, S. V, 2012. Viable Method for the Synthesis of Biphasic TiO 2 Nanocrystals with Tunable Phase Composition and Enabled Visible-Light Photocatalytic Performance. ACS applied materials & interfaces 4(3), 1239–1246. doi:10.1021/am201354r

Chandra Bhushan, 2006. The structure and economics of the Indian bottled water industry. Frontline Volume: 23. doi:http://www.frontline.in/static/html/fl2307/stories/20060421006702300.htm

Clifford, P., 2016. Type K Thermocouple Calibration [WWW Document]. Mosaic Industries, Inc. URL http://www.mosaic-industries.com/embedded-systems/microcontroller-projects/temperature-measurement/thermocouple/type-k-calibration-table (accessed 9.3.18).

Dashtban, M., Tabrizi, F.F., 2011. Thermal analysis of a weir-type cascade solar still integrated with PCM storage. Desalination 279, 415–422. doi:10.1016/j.desal.2011.06.044

Dsilva Winfred Rufuss, D., Iniyan, S., Davies, P.A., 2017a. Nanoparticles Enhanced Phase Change Material (NPCM) as Heat Storage in Solar Still Application for Productivity Enhancement. Energy Procedia 141, 45–49. doi:10.1016/j.egypro.2017.11.009

Dsilva Winfred Rufuss, D., Iniyan, S., Suganthi, L., 2018a. Combined Effect of Heat Storage, Reflective Material, and Additional Heat Source on the Productivity of a Solar Still—Techno-Economic Approach. Journal of Testing and Evaluation 46. doi:doi.org/10.1520/JTE20170013

Dsilva Winfred Rufuss, D., Iniyan, S., Suganthi, L., Davies, P.A., 2017b. Low mass fraction impregnation with graphene oxide (GO) enhances thermo-physical properties of paraffin for heat storage applications. Thermochimica Acta 655, 226–233. doi:10.1016/j.tca.2017.07.005

Dsilva Winfred Rufuss, D., Iniyan, S., Suganthi, L., Davies, P.A., 2016. Solar stills: A comprehensive review of designs, performance and material advances. Renewable and Sustainable Energy Reviews 63, 464–496. doi:10.1016/j.rser.2016.05.068

Dsilva Winfred Rufuss, D., Iniyan, S., Suganthi, L., Davies, P.A., Akinaga, T., 2015. Analysis of solar still with nanoparticle incorporated phase change material for solar desalination application, in: ISES Solar World Congress 2015. International Solar Energy Society, Daegu; South Korea, pp. 1271–1280. doi:10.18086/swc.2015.10.44

Dsilva Winfred Rufuss, D., Kumar, V.R., Suganthi, L., Iniyan, S., Davies, P.A., 2018b. Techno-economic analysis of solar stills using integrated fuzzy analytical hierarchy process and data envelopment analysis. Solar Energy 159, 820–833. doi:10.1016/j.solener.2017.11.050

El-Bialy, E., Shalaby, S.M., Kabeel, A.E., Fathy, A.M., 2016. Cost analysis for several solar desalination systems. Desalination 384, 12–30. doi:10.1016/j.desal.2016.01.028

El-Sebaii, A.A., Al-Ghamdi, A.A., Al-Hazmi, F.S., Faidah, A.S., 2009. Thermal performance of a single basin solar still with PCM as a storage medium. Applied Energy 86, 1187–1195. doi:10.1016/j.apenergy.2008.10.014

Eltawil, M.A., Omara, Z.M., 2014. Enhancing the solar still performance using solar photovoltaic, flat plate collector and hot air. Desalination 349, 1–9. doi:10.1016/j.desal.2014.06.021

Fang, G., Li, H., Yang, F., Liu, X., Wu, S., 2009. Preparation and characterization of nano-encapsulated n-tetradecane as phase change material for thermal energy storage. Chemical Engineering Journal 153, 217–221. doi:10.1016/j.cej.2009.06.019

Fath, H.E.S., El-Samanoudy, M., Fahmy, K., Hassabou, A., 2003. Thermal-economic analysis and comparison between pyramid-shaped and single-slope solar still configurations. Desalination 159, 69–79. doi:10.1016/S0011-9164(03)90046-4

Harikrishnan, S., Kalaiselvam, S., 2013. Experimental investigation of solidification and melting characteristics of nanofluid as PCM for solar water heating systems. International Journal of Emerging Technology and Advanced Engineering 3, 628–635.

Harikrishnan, S., Kalaiselvam, S., 2012. Preparation and thermal characteristics of CuO-oleic acid nanofluids as a phase change material. Thermochimica Acta 533, 46–55. doi:10.1016/j.tca.2012.01.018

Harikrishnan, S., Magesh, S., Kalaiselvam, S., 2013. Preparation and thermal energy storage behaviour of stearic acid-TiO 2 nanofluids as a phase change material for solar heating systems. Thermochimica Acta 565, 137–145. doi:10.1016/j.tca.2013.05.001

He, Q., Wang, S., Tong, M., Liu, Y., 2012. Experimental study on thermophysical properties of nanofluids as phase-change material (PCM) in low temperature cool storage. Energy Conversion and Management 64, 199–205. doi:10.1016/j.enconman.2012.04.010

Henisch, H.K., Roy, R., Leslie Eric Cross, E., 1973. Phase Transitions - 1973: Proceedings of the Conference on Phase Transitions and their Application in Material Science. Pergamon Press, Elsevier, University Park, Pennsylvania.

J.C. Jones, 1995. On the use of metal sheathed thermocouples in a hot gas layer originating from a room fire. Journal of Fire Sciences 13, 257–260. doi:https://doi.org/10.1177/073490419501300401

Jebasingh, B.E., 2016. Exfoliation of graphite by solar irradiation and investigate their thermal property on capric-myristic-palmitic acid/exfoliated graphite composite as phase change material (PCM) for energy storage. Journal of Energy Storage 5, 70–76. doi:10.1016/j.est.2015.11.004

Jegadheeswaran, S., Pohekar, S.D., 2009. Performance enhancement in latent heat thermal storage system: A review. Renewable and Sustainable Energy Reviews. doi:10.1016/j.rser.2009.06.024

Jubran, B.A., 2002. Effect of climatic , design and operational parameters on the yield of a simple solar still. Energy Conversion and Management 43, 1639–1650.

Kabeel, A.E., Abdelgaied, M., 2016. Improving the performance of solar still by using PCM as a thermal storage medium under Egyptian conditions. Desalination 383, 22–28. doi:10.1016/j.desal.2016.01.006

Kabeel, A.E., Abdelgaied, M., Eisa, A., 2018. Enhancing the performance of single basin solar still using high thermal conductivity sensible storage materials. Journal of Cleaner Production 183, 20–25. doi:10.1016/j.jclepro.2018.02.144

Kabeel, A.E., Abdelgaied, M., Mahgoub, M., 2016. The performance of a modified solar still

using hot air injection and PCM. Desalination 379, 102–107. doi:10.1016/j.desal.2015.11.007

Kabeel, A.E., El-Agouz, S.A., 2011. Review of researches and developments on solar stills. Desalination. doi:10.1016/j.desal.2011.03.042

Kabeel, A.E., El-maghlany, W.M., 2018. Comparative study on the solar still performance utilizing different PCM. Desalination 432, 89–96. doi:10.1016/j.desal.2018.01.016

Kabeel, A.E., Hamed, A.M., El-Agouz, S.A., 2010. Cost analysis of different solar still configurations. Energy 35, 2901–2908. doi:10.1016/j.energy.2010.03.021

Kabeel, A.E., Khalil, A., Omara, Z.M., Younes, M.M., 2012. Theoretical and experimental parametric study of modified stepped solar still. Desalination 289, 12–20. doi:10.1016/j.desal.2011.12.023

Kabeel, A.E., Omara, Z.M., Essa, F.A., Abdullah, A.S., Arunkumar, T., 2017. Augmentation of a solar still distillate yield via absorber plate coated with black nanoparticles. Alexandria Engineering Journal 56, 433–438. doi:10.1016/j.aej.2017.08.014

Kabeel, A.E., Teamah, M.A., Abdelgaied, M., Abdel Aziz, G.B., 2017. Modified pyramid solar still with v-corrugated absorber plate and PCM as a thermal storage medium. Journal of Cleaner Production 161, 881–887. doi:10.1016/j.jclepro.2017.05.195

Kalidasa Murugavel, K., Srithar, K., 2011. Performance study on basin type double slope solar still with different wick materials and minimum mass of water. Renewable Energy 36, 612–620. doi:10.1016/j.renene.2010.08.009

Khodadadi, J.M., Hosseinizadeh, S.F., 2007. Nanoparticle-enhanced phase change materials (NEPCM) with great potential for improved thermal energy storage. International Communications in Heat and Mass Transfer 34, 534–543. doi:10.1016/j.icheatmasstransfer.2007.02.005

Khoshvaght-aliabadi, M., Hormozi, F., Zamzamian, A., 2014. Experimental analysis of thermal – hydraulic performance of copper – water nanofluid flow in different plate-fin channels. Experimental Thermal and Fluid Science 52, 248–258. doi:10.1016/j.expthermflusci.2013.09.018

Kumar, P.V., 2015. Enhanced Electrical, Optical and Chemical Properties of Graphene Oxide through a Novel Phase Transformation, in: Doctoral dissertation,Indian Institute of Technology Madras,. pp. 1–106.

Kumar, S., Tiwari, G.N., 1996. Estimation of convective mass transfer in solar distillation systems. Solar Energy 57, 459–464. doi:10.1016/S0038-092X(96)00122-3

Kundu, S., Das, A., Basu, A., Abdullah, F., Mukherjee, A., 2017. Guar gum benzoate nanoparticle reinforced gelatin films for enhanced thermal insulation , mechanical and antimicrobial properties. Carbohydrate Polymers 170, 89–98. doi:10.1016/j.carbpol.2017.04.056

Lee, D., Kim, J., Kim, B.G., 2006. A New Parameter to Control Heat Transport in Nanofluids : Surface Charge State of the Particle in Suspension. The Journal of Physical Chemistry B 110, 4323–4328. doi:10.1021/jp057225m

Linseis, 1957. Linseis thermal analysis [WWW Document]. [https://www.linseis.com/en/our-products/thermal-diffusivity-thermal-conductivity/lfa-1000-laser-flash/.

Lokesh.S, Murugan.P, Sathishkumar.A, Kumaresan.V, Velraj.R, 2015. Melting/solidification characteristics of paraffin based nanocomposite for thermal energy storage applications. Thermal Science 170.

Lotfizadehdehkordi, B., Kazi, S.N., Hamdi, M., Ghadimi, A., Sadeghinezhad, E., Metselaar, H.S.C., 2013. Investigation of viscosity and thermal conductivity of alumina nanofluids with addition of SDBS. Heat Mass Transfer 49, 1109–1115. doi:10.1007/s00231-013-1153-8

Mahian, O., Kianifar, A., Zeinali, S., Wen, D., Sahin, A.Z., 2017. Nanofluids effects on the evaporation rate in a solar still equipped with a heat exchanger. Nano Energy 36, 134–155. doi:10.1016/j.nanoen.2017.04.025

Malik, S., Vijayaraghavan, A., Erni, R., Ariga, K., De, I.K., Hill, J.P., 2010. High purity graphenes prepared by a chemical intercalation method. Nanoscale 2(10), 2139–2143. doi:10.1039/c0nr00248h

Manivel, R., Sivakumar, S., Dsilva Winfred Rufuss, D., 2014. Experimental Investigation of

Solar Desalination System with Roof Heating. International Journal of Earth Sciences and Engineering 7, 1459–1464. doi:http://cafetinnova.org/innova/archiveList/IJEE/2014/04/02070433.htm?paperID=1270

Manokar, A.M., Winston, D.P., Kabeel, A.E., Sathyamurthy, R., 2018. Sustainable fresh water and power production by integrating PV panel in inclined solar still. Journal of Cleaner Production 172, 2711–2719. doi:10.1016/j.jclepro.2017.11.140

Mehrali, M., Latibari, S.T., Mehrali, M., Simon, H., Metselaar, C., 2013. Shape-stabilized phase change materials with high thermal conductivity based on paraffin / graphene oxide composite. Energy Conversion and Management 67, 275–282. doi:10.1016/j.enconman.2012.11.023

Mkhoyan, K.A., Contryman, A.W., Silcox, J., Stewart, D.A., Eda, G., Mattevi, C., Miller, S., 2009. Atomic and Electronic Structure of Graphene-Oxide. Nano letters 9(3), 1058–1063.

Motahar, S., Nikkam, N., Alemrajabi, A.A., Khodabandeh, R., Toprak, M.S., Muhammed, M., 2014. Experimental investigation on thermal and rheological properties of n-octadecane with dispersed TiO2 nanoparticles. International Communications in Heat and Mass Transfer 59, 68–74. doi:10.1016/j.icheatmasstransfer.2014.10.016

Mousa, H., Gujarathi, A.M., 2016. Modeling and analysis the productivity of solar desalination units with phase change materials. Renewable Energy 95, 225–232. doi:10.1016/j.renene.2016.04.013

Muftah, A.F., Alghoul, M.A., Fudholi, A., Abdul-Majeed, M.M., Sopian, K., 2014. Factors affecting basin type solar still productivity: A detailed review. Renewable and Sustainable Energy Reviews. doi:10.1016/j.rser.2013.12.052

Murugavel, K.K., Sivakumar, S., Ahamed, J.R., Chockalingam, K.K.S.K., Srithar, K., 2010. Single basin double slope solar still with minimum basin depth and energy storing materials. Applied Energy 87, 514–523. doi:10.1016/j.apenergy.2009.07.023

NIST ITS-90 Thermocouple Database, 1993. NIST ITS-90 Thermocouple Database. National Institute of Standards and Technology (NIST) Monograph 175, 630. doi:https://srdata.nist.gov/its90/main/

O'Neill, M., 1966. Measurement of Specific Heat Functions by Differential Scanning Calorimetry. Analytical chemistry 38, 1331–1336.

Omara, Z.M., Kabeel, A.E., Essa, F.A., 2015. Effect of using nanofluids and providing vacuum on the yield of corrugated wick solar still. Energy Conversion and Management 103, 965–972. doi:10.1016/j.enconman.2015.07.035

Parameshwaran, R., Kalaiselvam, S., Harikrishnan, S., Elayaperumal, A., 2012. Sustainable thermal energy storage technologies for buildings: A review. Renewable and Sustainable Energy Reviews. doi:10.1016/j.rser.2012.01.058

Pei, S., Cheng, H., 2011. The reduction of graphene oxide. Carbon 50, 3210–3228. doi:10.1016/j.carbon.2011.11.010

Prakash, P., Velmurugan, V., 2015. Parameters influencing the productivity of solar stills – A review. Renewable and Sustainable Energy Reviews 49, 585–609. doi:10.1016/j.rser.2015.04.136

Rajaseenivasan, T., Tinnokesh, A.P., Kumar, G.R., Srithar, K., 2016. Glass basin solar still with integrated preheated water supply ??? Theoretical and experimental investigation. Desalination 398, 214–221. doi:10.1016/j.desal.2016.07.041

Ranjan, K.R., Kaushik, S.C., 2013. Economic feasibility evaluation of solar distillation systems based on the equivalent cost of environmental degradation and high-grade energy savings. International Journal of Low-Carbon Technologies 11, 8–15. doi:doi.org/10.1093/ijlct/ctt048

Renteria, J.D., Ramirez, S., Malekpour, H., Alonso, B., Centeno, A., Zurutuza, A., Cocemasov, A.I., Nika, D.L., Balandin, A.A., 2015. Strongly Anisotropic Thermal Conductivity of Free-Standing Reduced Graphene Oxide Films Annealed at High Temperature. Advanced Functional Materials 25, 4664–4672. doi:10.1002/adfm.201501429

Sadhasivam, B., Rigana, M.F., 2018. Chiral polyimide and its nanocomposites with graphene oxide using L -phenylalanine-based diamine. Polymer Bulletin 75, 829–849. doi:10.1007/s00289-017-2050-y

Sakthivel, M., Shanmugasundaram, S., 2008. Effect of energy storage medium (black granite

gravel) on the performance of a solar still. International Journal of Energy Research 32, 68–82. doi:10.1002/er.1335

Sakthivel, M., Shanmugasundaram, S., Alwarsamy, T., 2010. An experimental study on a regenerative solar still with energy storage medium - Jute cloth. Desalination 264, 24–31. doi:10.1016/j.desal.2010.06.074

Samuel, D.G.H., Nagarajan, P.K., Sathyamurthy, R., El-agouz, S.A., Kannan, E., 2016. Improving the yield of fresh water in conventional solar still using low cost energy storage material. Energy Conversion and Management 112, 125–134. doi:10.1016/j.enconman.2015.12.074

Sandeep, Kumar, S., Dwivedi, V.K., 2015. Experimental study on modified single slope single basin active solar still. Desalination 367, 69–75. doi:doi.org/10.1016/j.desal.2015.03.031

Sari, A., Karaipekli, A., 2007. Thermal conductivity and latent heat thermal energy storage characteristics of paraffin/expanded graphite composite as phase change material. Applied Thermal Engineering 27, 1271–1277. doi:10.1016/j.applthermaleng.2006.11.004

Sciacovelli, A., Colella, F., Verda, V., 2013. Melting of PCM in a thermal energy storage unit: Numerical investigation and effect of nanoparticle enhancement. International Journal of Energy Research 37, 1610–1623. doi:10.1002/er.2974

Shalaby, S.M., El-Bialy, E., El-Sebaii, A.A., 2016. An experimental investigation of a v-corrugated absorber single-basin solar still using PCM. Desalination 398, 247–255. doi:10.1016/j.desal.2016.07.042

Shanmugan, S., Janarthanan, B., Chandrasekaran, J., 2012. Performance of single-slope single-basin solar still with sensible heat storage materials. Desalination and Water Treatment 41, 195–203. doi:10.1080/19443994.2012.664714

Shannon, K.S., Butler, B.W., 2003. A review of error associated with thermocouple temperature measurement in fire environments, in: Second International Wildland Fire Ecology an Fire Management Congress and Fifth Symposium on Fire and Forest Meteorology, American Meteorological Society, Orlando, Fl. Boston, MA (2003). p. 7B.4.3p.

Sharma, A., Sharma, S.D., Buddhi, D., 2002. Accelerated thermal cycle test of acetamide, stearic acid and paraffin wax for solar thermal latent heat storage applications. Energy Conversion and Management 43, 1923–1930. doi:10.1016/S0196-8904(01)00131-5

Sharma, M., Singh, A.K., Yadav, D.N., Arora, S., Vishwakarma, R.K., 2016. Impact of octenyl succinylation on rheological , pasting , thermal and physicochemical properties of pearl millet (Pennisetum typhoides) starch. LWT - Food Science and Technology 73, 52–59. doi:10.1016/j.lwt.2016.05.034

Sharma, R.K., Ganesan, P., Tyagi, V. V., Metselaar, H.S.C., Sandaran, S.C., 2016. Thermal properties and heat storage analysis of palmitic acid-TiO2 composite as nano-enhanced organic phase change material (NEOPCM). Applied Thermal Engineering 99, 1254–1260. doi:10.1016/j.applthermaleng.2016.01.130

Sharma, S., Micheli, L., Chang, W., Tahir, A.A., Reddy, K.S., Mallick, T.K., 2017. Nano-enhanced Phase Change Material for thermal management of BICPV. Applied Energy 208, 719–733. doi:10.1016/j.apenergy.2017.09.076

Sharshir, S.W., Yang, N., Peng, G., Kabeel, A.E., 2016. Factors affecting solar stills productivity and improvement techniques: A detailed review. Applied Thermal Engineering 100, 267–284. doi:10.1016/j.applthermaleng.2015.11.041

Sheng, Z., Shao, L., Chen, J., Bao, W., Wang, F., Xia, X., 2011. Catalyst-Free Synthesis of Nitrogen- Doped Graphene via Thermal Annealing Graphite Oxide with Melamine and Its Excellent Electrocatalysis. ACS nano 5, 4350–4358. doi:10.1021/nn103584t

Shi, J., Ger, M., Liu, Y., Fan, Y., Wen, N., Lin, C., Pu, N., 2012. Improving the thermal conductivity and shape-stabilization of phase change materials using nanographite additives. Carbon 51, 365–372. doi:10.1016/j.carbon.2012.08.068

Silakhori, M., Naghavi, M.S., Simon, H., Metselaar, C., Meurah, T., Mahlia, I., Fauzi, H., Mehrali, M., 2013. Accelerated Thermal Cycling Test of Microencapsulated Paraffin Wax/Polyaniline Made by Simple Preparation Method for Solar Thermal Energy Storage. materials 6, 1608–1620. doi:10.3390/ma6051608

Sohail, M., Saleem, M., Ullah, S., Saeed, N., Afridi, A., Khan, M., Arif, M., 2017. Modified

and improved Hummer ’s synthesis of graphene oxide for capacitors applications. Modern Electronic Materials 3, 110–116. doi:10.1016/j.moem.2017.07.002

Somanchi, N.S., B, A.P., Gugulothu, R., Nagula, R.K., K, S.P.D., 2015. Performance of Solar Still with Different Phase Change Materials. International Journal of Energy and Power Engineering 4, 33–37. doi:10.11648/j.ijepe.s.2015040501.15

Suchitra, M., 2004. Thermal Analysis of Composites Using DSC. Advanced topics in characterization of composites 11–33.

Swetha, K., Venugopal, J., 2011. Experimental investigation of a single slope solar still using PCM. International Journal of Research in Environmental Science and technology 1, 30–33.

Tabrizi, F.F., Dashtban, M., Moghaddam, H., 2010. Experimental investigation of a weir-type cascade solar still with built-in latent heat thermal energy storage system. Desalination 260, 248–253. doi:10.1016/j.desal.2010.03.033

Tang, Y., Su, D., Huang, X., Alva, G., Liu, L., Fang, G., 2016. Synthesis and thermal properties of the MA/HDPE composites with nano-additives as form-stable PCM with improved thermal conductivity. Applied Energy 180, 116–129. doi:10.1016/j.apenergy.2016.07.106

Tiwari G N, Khan M E, G.R.K., 1998. Experimental study of evaporation in distillation. Desalination 115, 121–128. doi:https://doi.org/10.1016/S0011-9164(98)00031-9

Velmurugan, V., Deenadayalan, C.K., Vinod, H., Srithar, K., 2008a. Desalination of effluent using fin type solar still. Energy 33, 1719–1727. doi:10.1016/j.energy.2008.07.001

Velmurugan, V., Gopalakrishnan, M., Raghu, R., Srithar, K., 2008b. Single basin solar still with fin for enhancing productivity. Energy Conversion and Management 49, 2602–2608. doi:10.1016/j.enconman.2008.05.010

Velmurugan, V., Naveen Kumar, K.J., Noorul Haq, T., Srithar, K., 2009. Performance analysis in stepped solar still for effluent desalination. Energy 34, 1179–1186. doi:10.1016/j.energy.2009.04.029

Viet, T., Hung, V., Trung, Q., Hong, S., Suk, J., 2010. Photoluminescence and Raman studies of graphene thin fi lms prepared by reduction of graphene oxide. Materials Letters 64, 399–401. doi:10.1016/j.matlet.2009.11.029

Wang, J., Li, Z., Fan, G., Pan, H., Zhang, D., 2012. Reinforcement with graphene nanosheets in aluminum matrix composites. Scripta Materialia 66, 594–597. doi:10.1016/j.scriptamat.2012.01.012

Yang, Y., Luo, J., Song, G., Liu, Y., Tang, G., 2014. The experimental exploration of nano-Si3N4/paraffin on thermal behavior of phase change materials. Thermochimica Acta 597, 101–106. doi:10.1016/j.tca.2014.10.014

Yu, W., Xie, H., Bao, D., 2010. Enhanced thermal conductivities of nanofluids containing graphene oxide nanosheets. Nanotechnology 21, 55705. doi:10.1088/0957-4484/21/5/055705

Zhang, H., Banfield, J.F., 2000. Understanding Polymorphic Phase Transformation Behavior during Growth of Nanocrystalline Aggregates : Insights from TiO 2. The Journal of Physical Chemistry B 104, 3481–3487. doi:10.1021/jp000499j

Zhao, B., Liu, P., Jiang, Y., Pan, D., Tao, H., Song, J., Fang, T., Xu, W., 2012. Supercapacitor performances of thermally reduced graphene oxide. Journal of Power Sources 198, 423–427. doi:10.1016/j.jpowsour.2011.09.074

List of Table caption

List of Figures caption

Fig. 11. Comparison of hourly yield for SSPCM, SSNPCM-1, SSNPCM-2 and SSNPCM-3

Fig. 12. Cumulative daily yield of SSPCM, SSNPCM-1, SSNPCM-2 and SSNPCM-3

Fig. 13. Hourly variation of solar intensity and wind velocity

Fig. 14. Comparison of water temperatures of SSPCM, SSNPCM-1, SSNPCM-2 and SSNPCM-3

Fig. 15. Comparison of absorber plate temperatures of SSPCM, SSNPCM-1, SSNPCM-2 and SSNPCM-3

Fig. 16. Temperatures in storage unit of SSPCM, SSNPCM-1, SSNPCM-2 and SSNPCM-3

Fig. 17. Water and glass cover temperature difference in SSPCM, SSNPCM-1, SSNPCM-2 and SSNPCM-3

Fig. 18. Overall comparison of various parameters for SSPCM, SSNPCM-1, SSNPCM-2 and SSNPCM-3

Highlights

1. TiO_2, CuO and GO nanoparticles are used to enhance the PCM properties
2. Thermal conductivity,latent heat,melting and solidification properties are studied
3. Techno-economic viability of solar stills with such nano-PCM is investigated
4. Still with paraffin+CuO gives highest yield of 5.28 l/m^2day with lowest water cost
5. This still produces water at $0.026/l ie. less than half the cost of bottled water

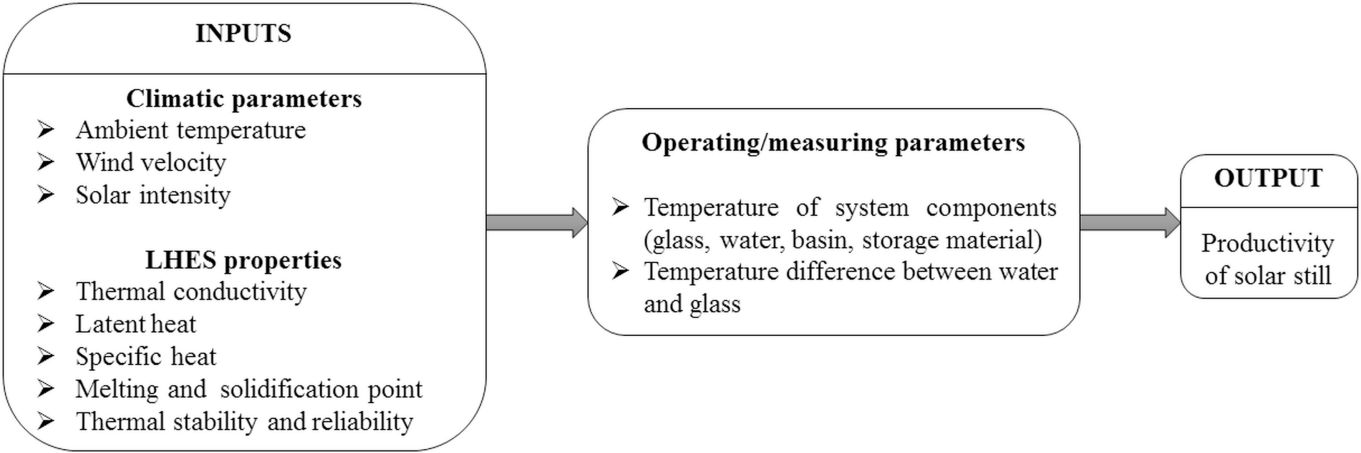
INPUTS
Climatic parameters
Ambient temperature
Wind velocity
Solar intensity
LHES properties
Thermal conductivity
Latent heat
Specific heat
Melting and solidification point
Thermal stability and reliability
Operating/measuring parameters
Temperature of system components (glass, water, basin, storage material)
Temperature difference between water and glass
OUTPUT
Productivity of solar still

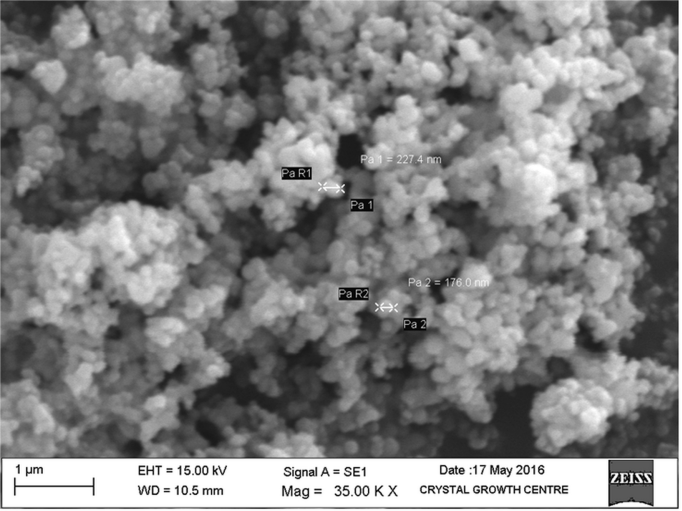

a. TiO_2

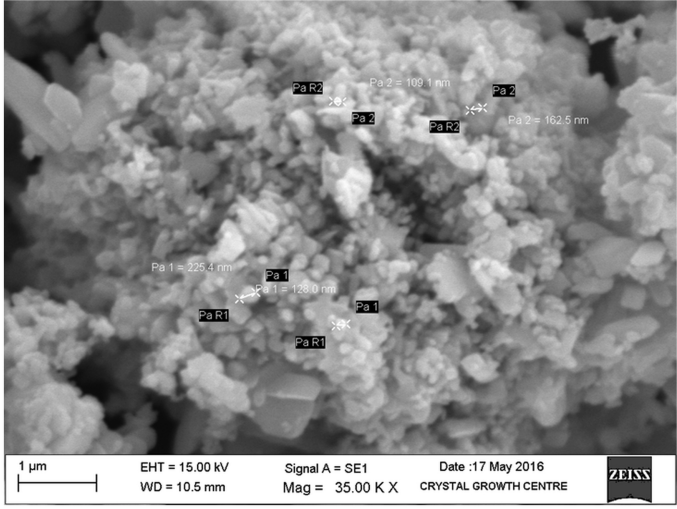

b. CuO

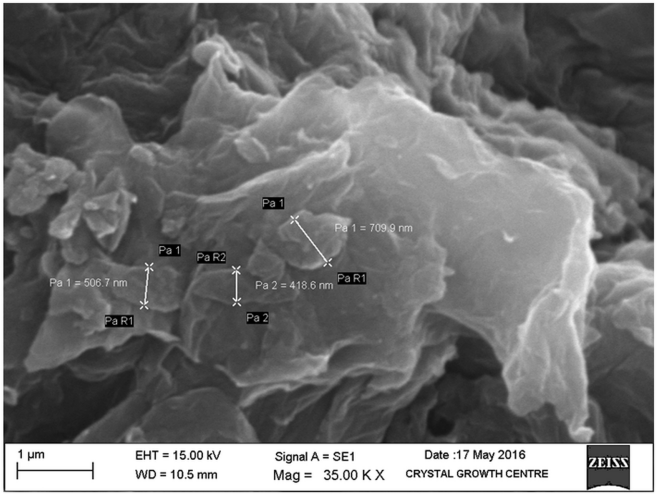

c. GO

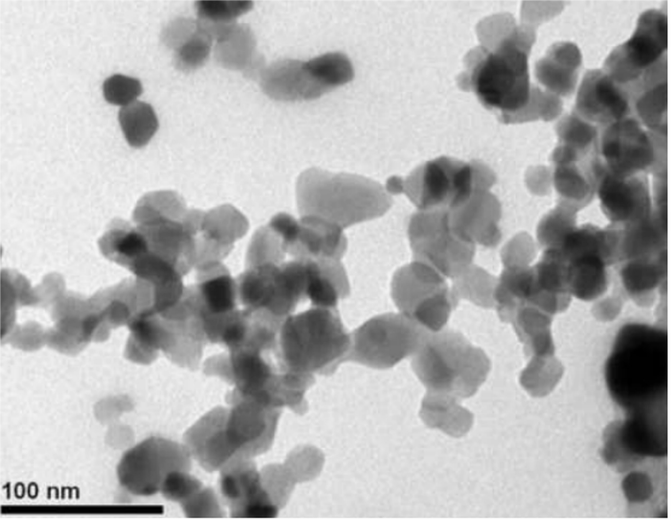

a. TiO_2

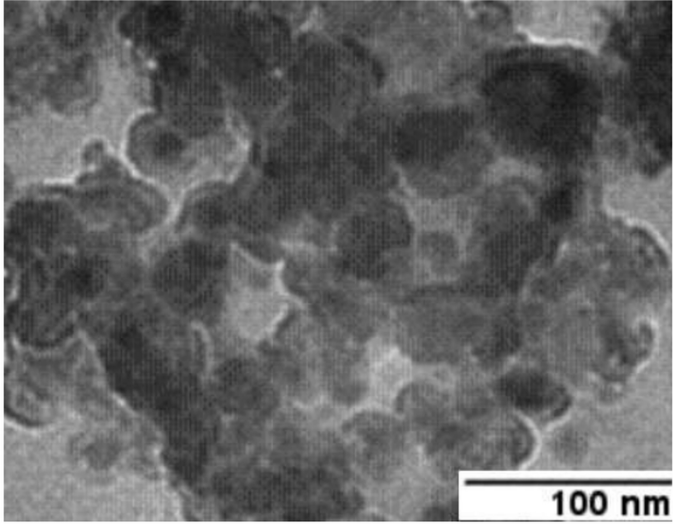

b. CuO

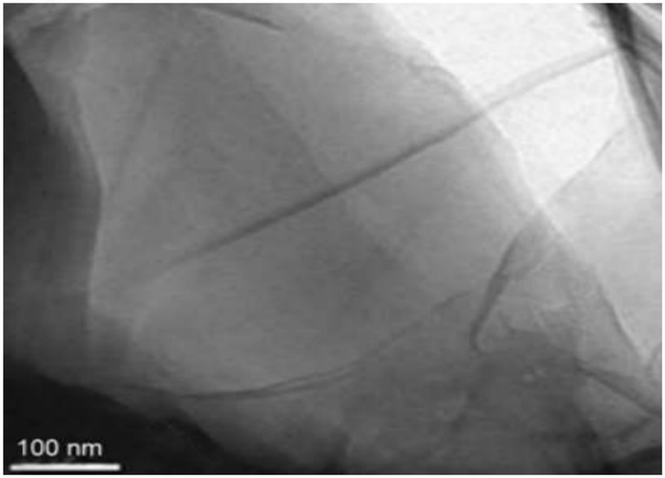

c. GO

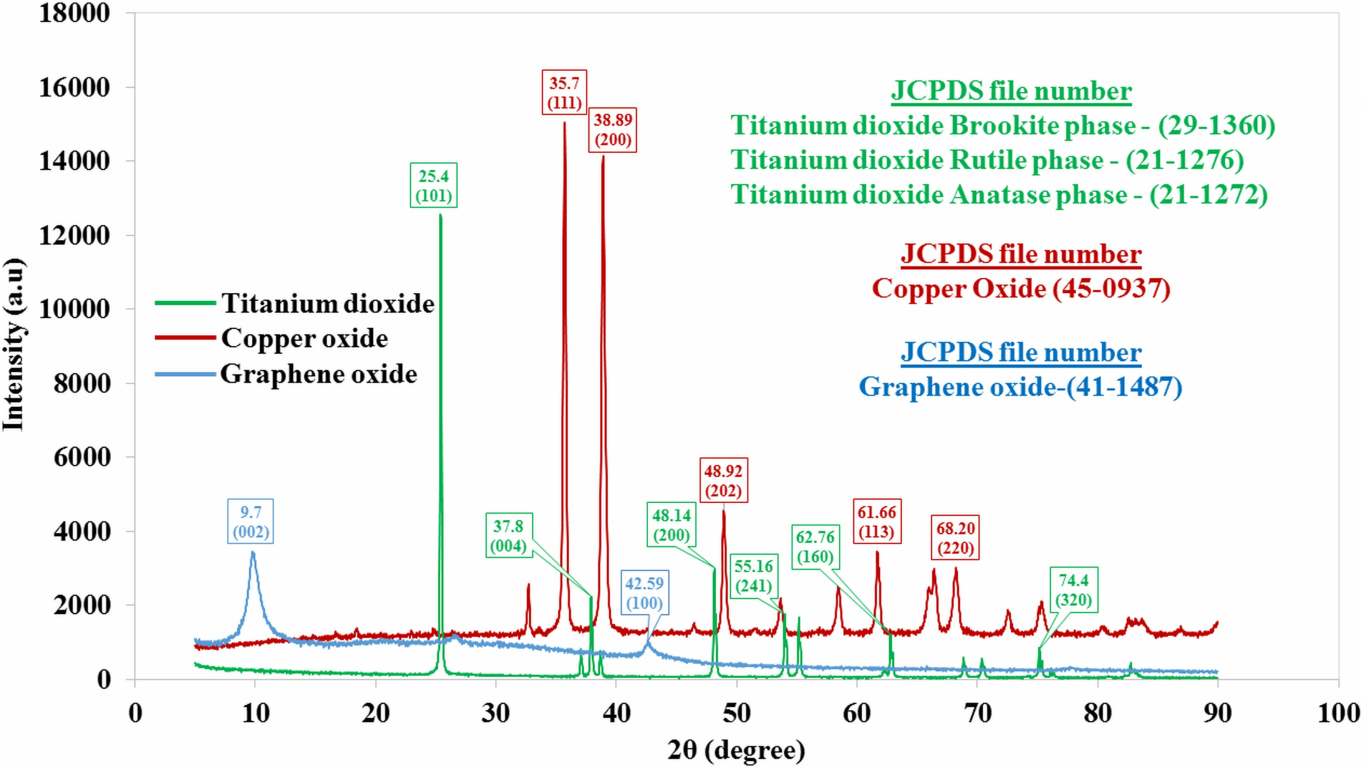
JCPDS file number
Titanium dioxide Brookite phase - (29-1360)
Titanium dioxide Rutile phase - (21-1276)
Titanium dioxide Anatase phase - (21-1272)
JCPDS file number
Copper Oxide (45-0937)
JCPDS file number
Graphene oxide-(41-1487)
Titanium dioxide
Copper oxide
Graphene oxide
9.7 (002)
25.4 (101)
37.8 (004)
35.7 (111)
38.89 (200)
42.59 (100)
48.14 (200)
48.92 (202)
55.16 (241)
62.76 (160)
61.66 (113)
68.20 (220)
74.4 (320)
Intensity (a.u)
2θ (degree)
0
2000
4000
6000
8000
10000
12000
14000
16000
18000
0
10
20
30
40
50
60
70
80
90
100

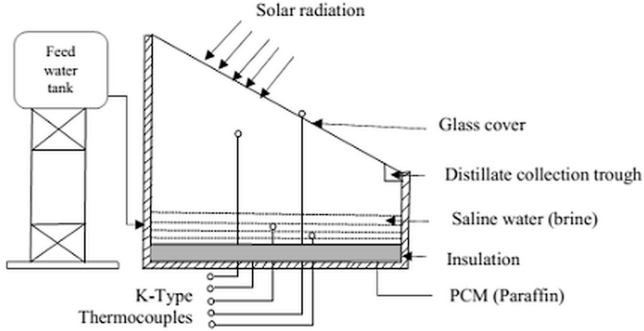

a. Solar still with PCM (Paraffin)

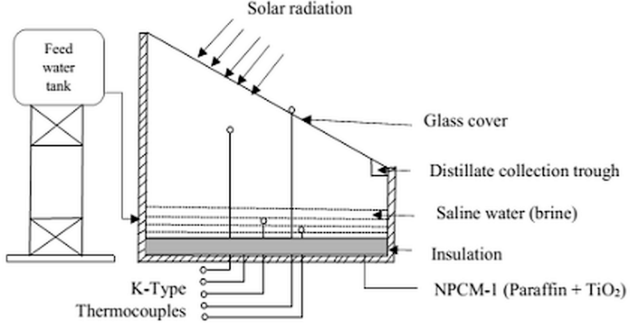

b. Solar still with NPCM-1 (Paraffin + TiO_2)

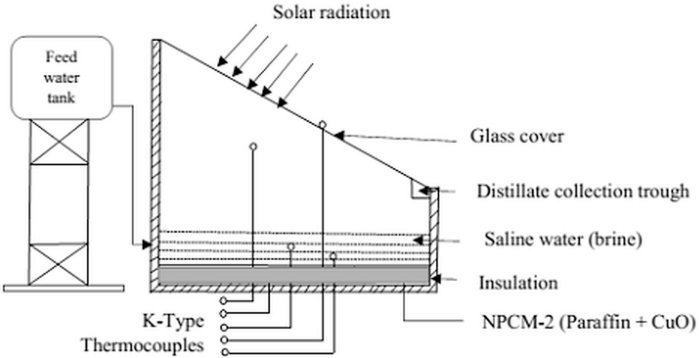

c. Solar still with NPCM-2 (Paraffin + CuO)

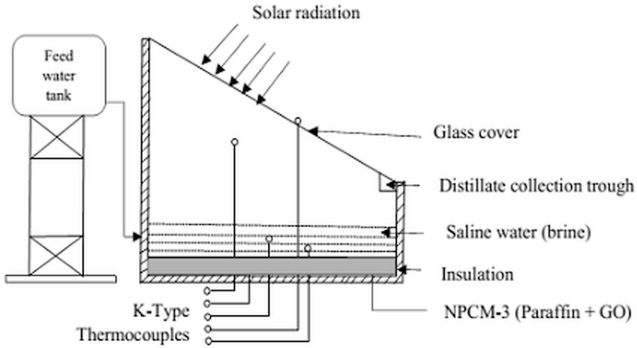

d. Solar still with NPCM-3 (Paraffin + GO)


SSNPCM-1
SSPCM
SSNPCM-2
SSNPCM-3

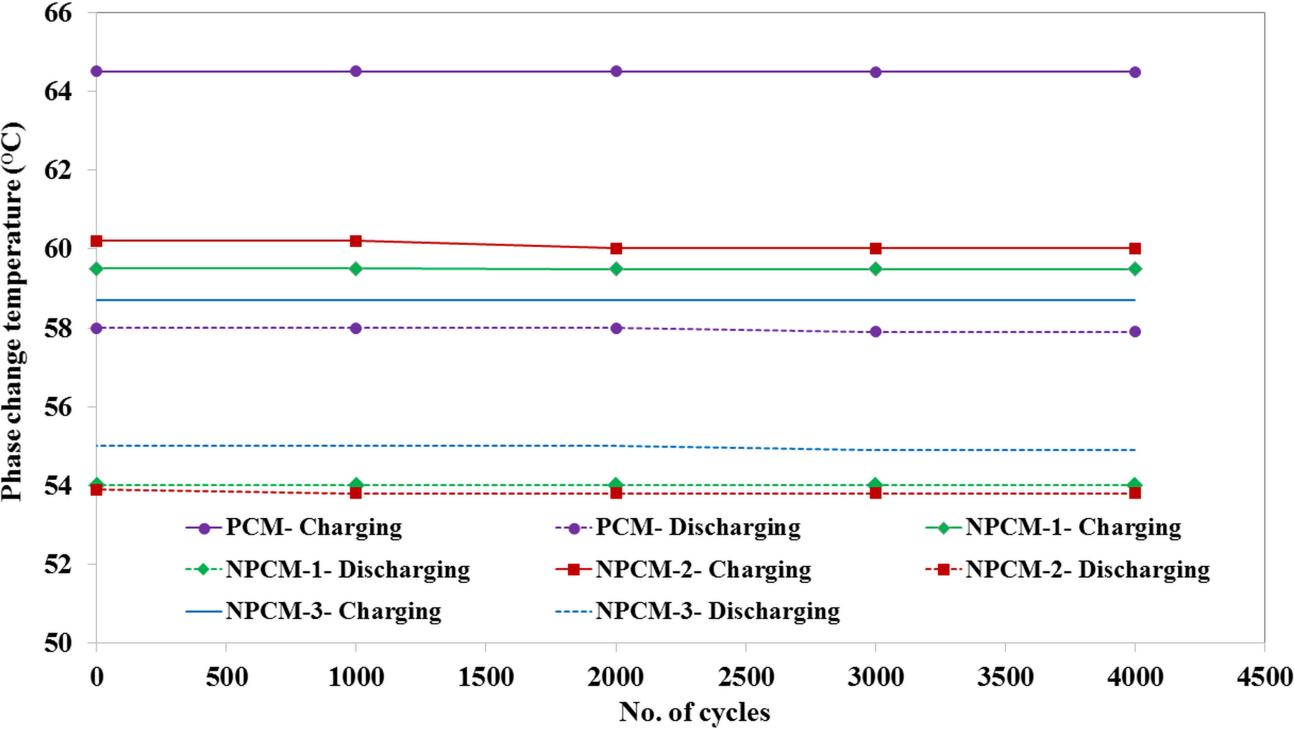
66
64
62
60
58
56
54
52
50
Phase change temperature (°C)
0
500
1000
1500
2000
2500
3000
3500
4000
4500
No. of cycles
PCM- Charging
PCM- Discharging
NPCM-1- Charging
NPCM-1- Discharging
NPCM-2- Charging
NPCM-2- Discharging
NPCM-3- Charging
NPCM-3- Discharging

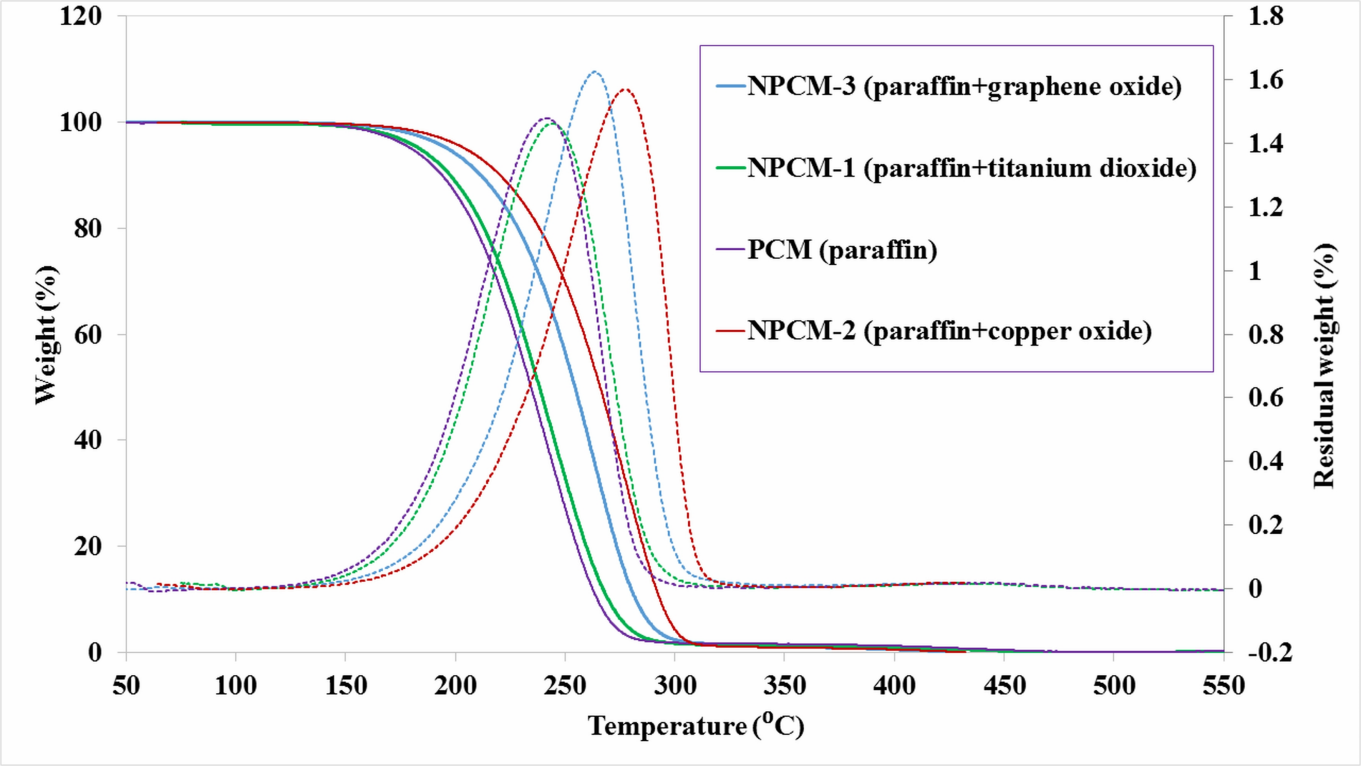
NPCM-3 (paraffin+graphene oxide)
NPCM-1 (paraffin+titanium dioxide)
PCM (paraffin)
NPCM-2 (paraffin+copper oxide)
Weight (%)
Residual weight (%)
Temperature (°C)
120
100
80
60
40
20
0
1.8
1.6
1.4
1.2
1
0.8
0.6
0.4
0.2
0
-0.2
50
100
150
200
250
300
350
400
450
500
550

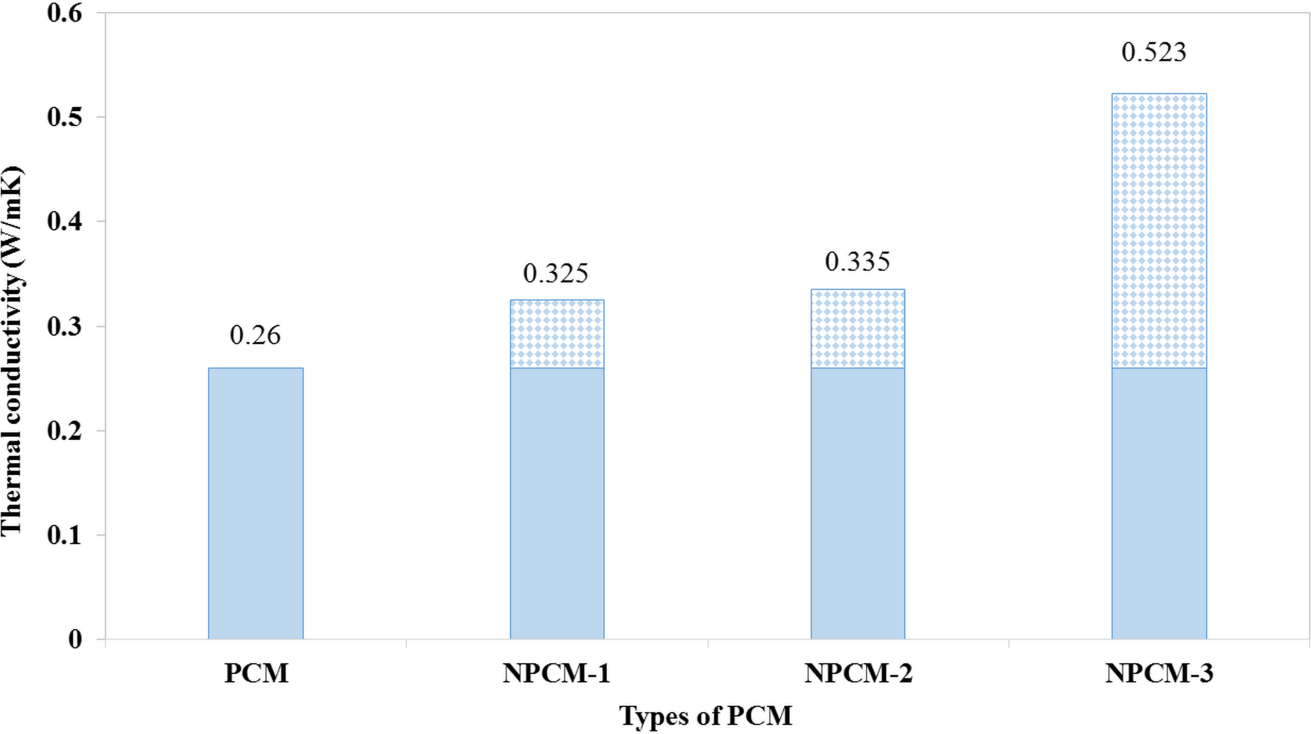
0.6
0.5
0.4
0.3
0.2
0.1
0
Thermal conductivity (W/mK)
0.26
0.325
0.335
0.523
PCM
NPCM-1
NPCM-2
NPCM-3
Types of PCM

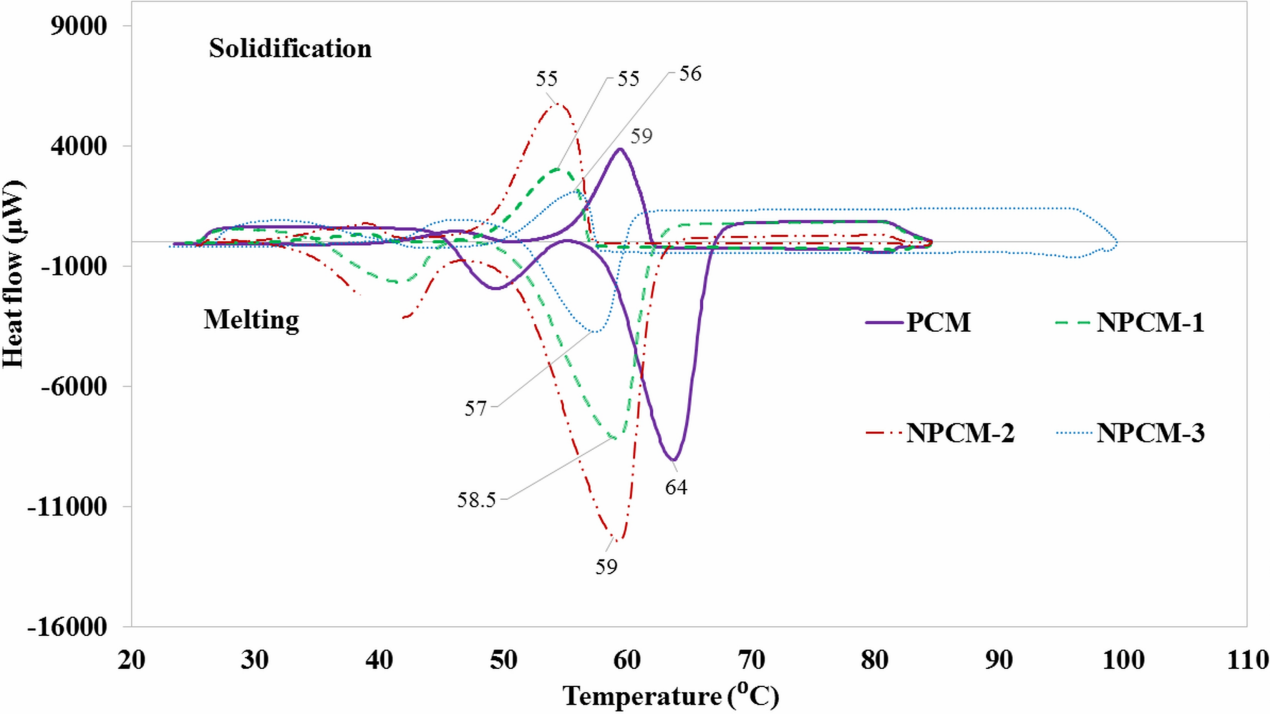
Solidification
Melting
55
55
56
59
57
58.5
59
64
PCM
NPCM-1
NPCM-2
NPCM-3
Heat flow (µW)
9000
4000
-1000
-6000
-11000
-16000
20
30
40
50
60
70
80
90
100
110
Temperature (⁰C)

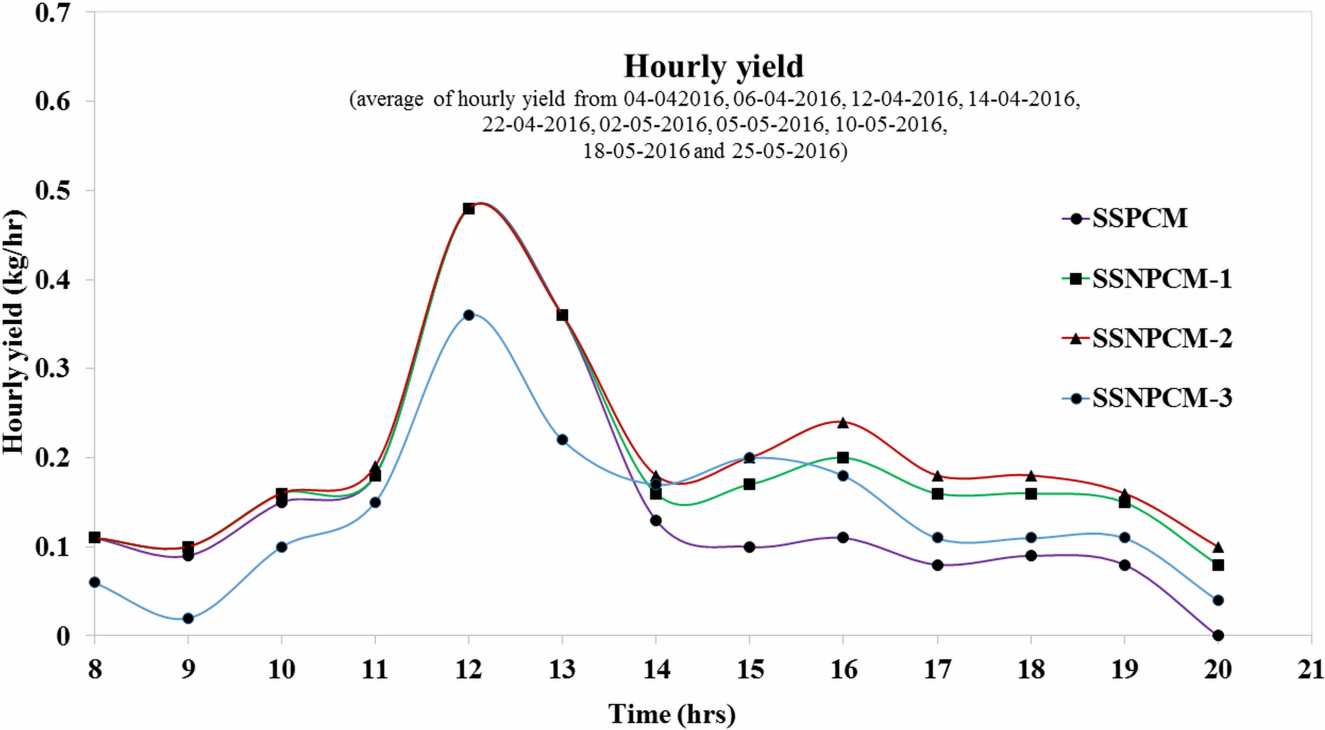
Hourly yield
(average of hourly yield from 04-042016, 06-04-2016, 12-04-2016, 14-04-2016, 22-04-2016, 02-05-2016, 05-05-2016, 10-05-2016, 18-05-2016 and 25-05-2016)
SSPCM
SSNPCM-1
SSNPCM-2
SSNPCM-3
Hourly yield (kg/hr)
0.7
0.6
0.5
0.4
0.3
0.2
0.1
0
8
9
10
11
12
13
14
15
16
17
18
19
20
21
Time (hrs)

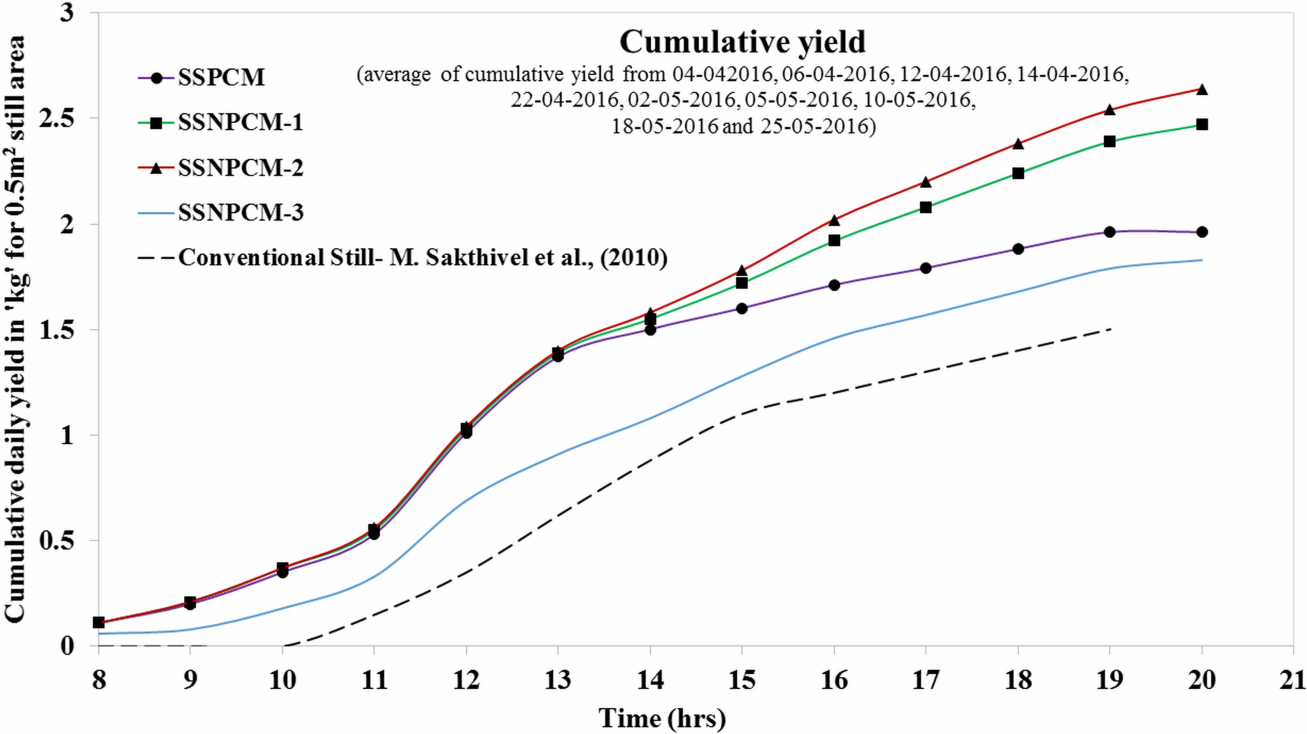
Cumulative yield
(average of cumulative yield from 04-042016, 06-04-2016, 12-04-2016, 14-04-2016, 22-04-2016, 02-05-2016, 05-05-2016, 10-05-2016, 18-05-2016 and 25-05-2016)
SSPCM
SSNPCM-1
SSNPCM-2
SSNPCM-3
Conventional Still- M. Sakthivel et al., (2010)
Cumulative daily yield in 'kg' for 0.5m2 still area
Time (hrs)
0
0.5
1
1.5
2
2.5
3
8
9
10
11
12
13
14
15
16
17
18
19
20
21

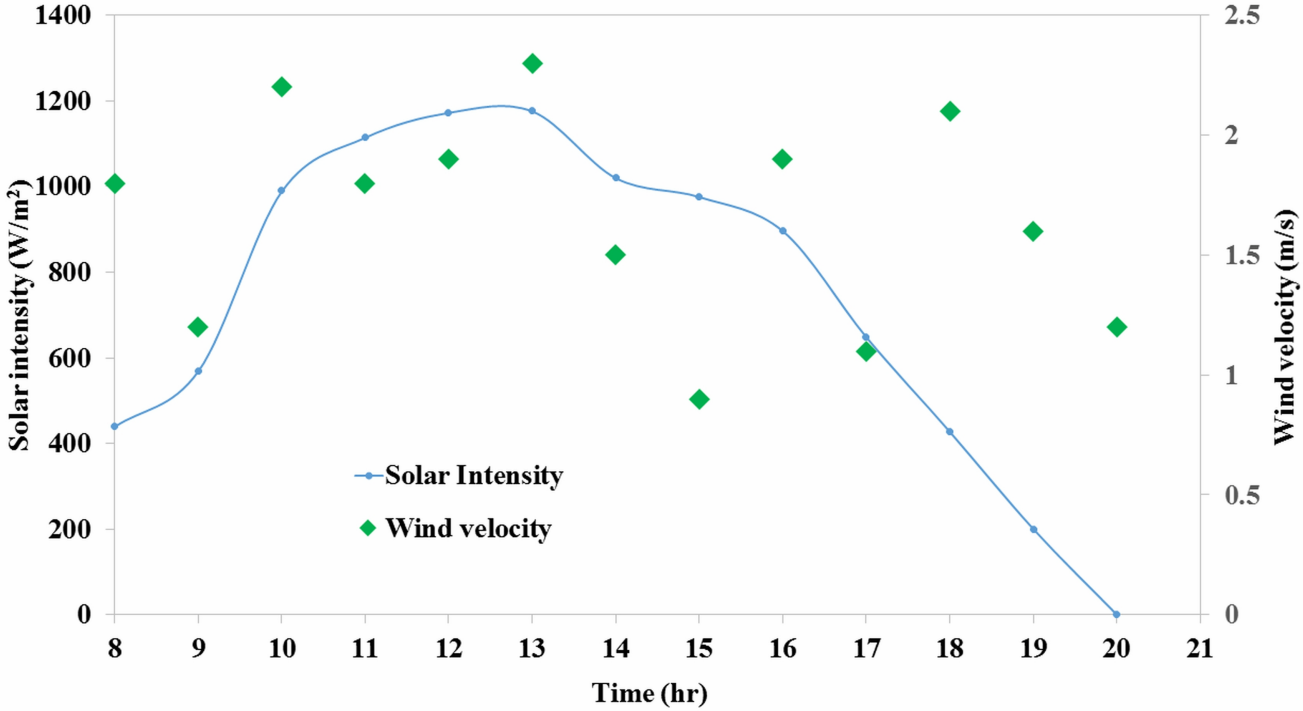
1400
1200
1000
800
600
400
200
0
Solar intensity (W/m²)
2.5
2
1.5
1
0.5
0
Wind velocity (m/s)
8
9
10
11
12
13
14
15
16
17
18
19
20
21
Time (hr)
Solar Intensity
Wind velocity

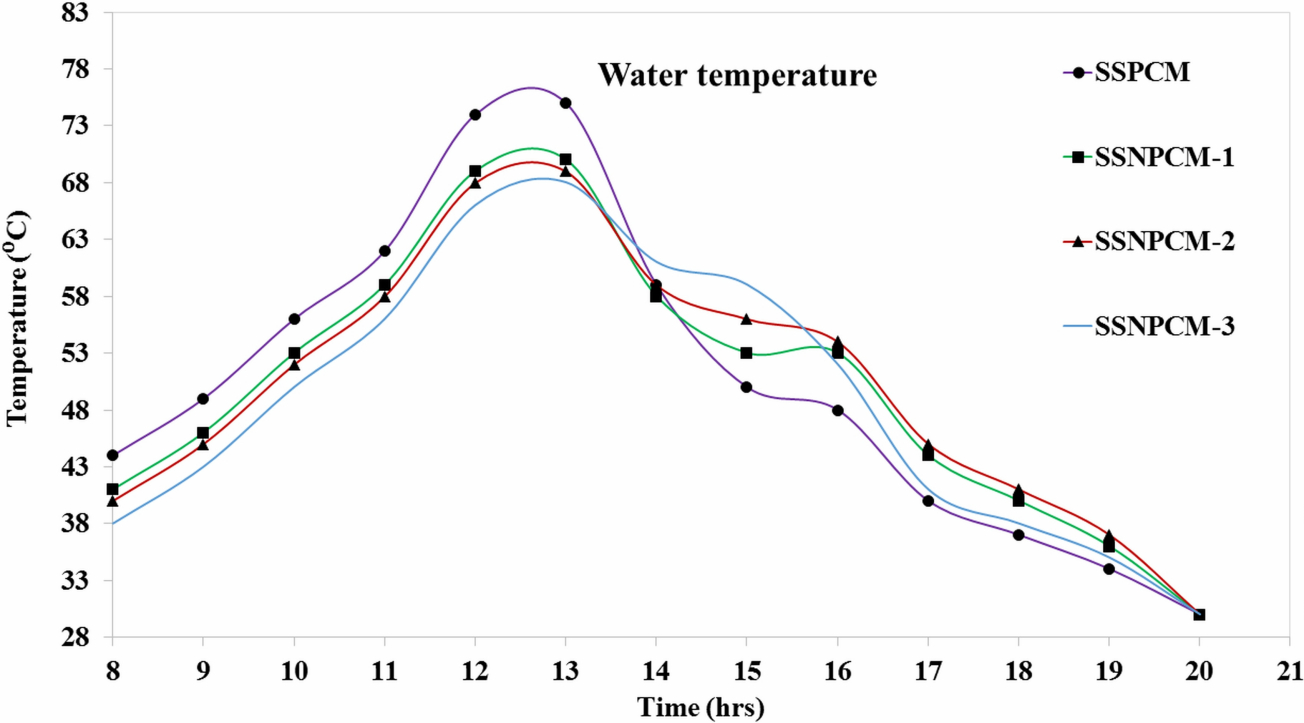
Water temperature
SSPCM
SSNPCM-1
SSNPCM-2
SSNPCM-3
Temperature (°C)
Time (hrs)
83
78
73
68
63
58
53
48
43
38
33
28
8
9
10
11
12
13
14
15
16
17
18
19
20
21

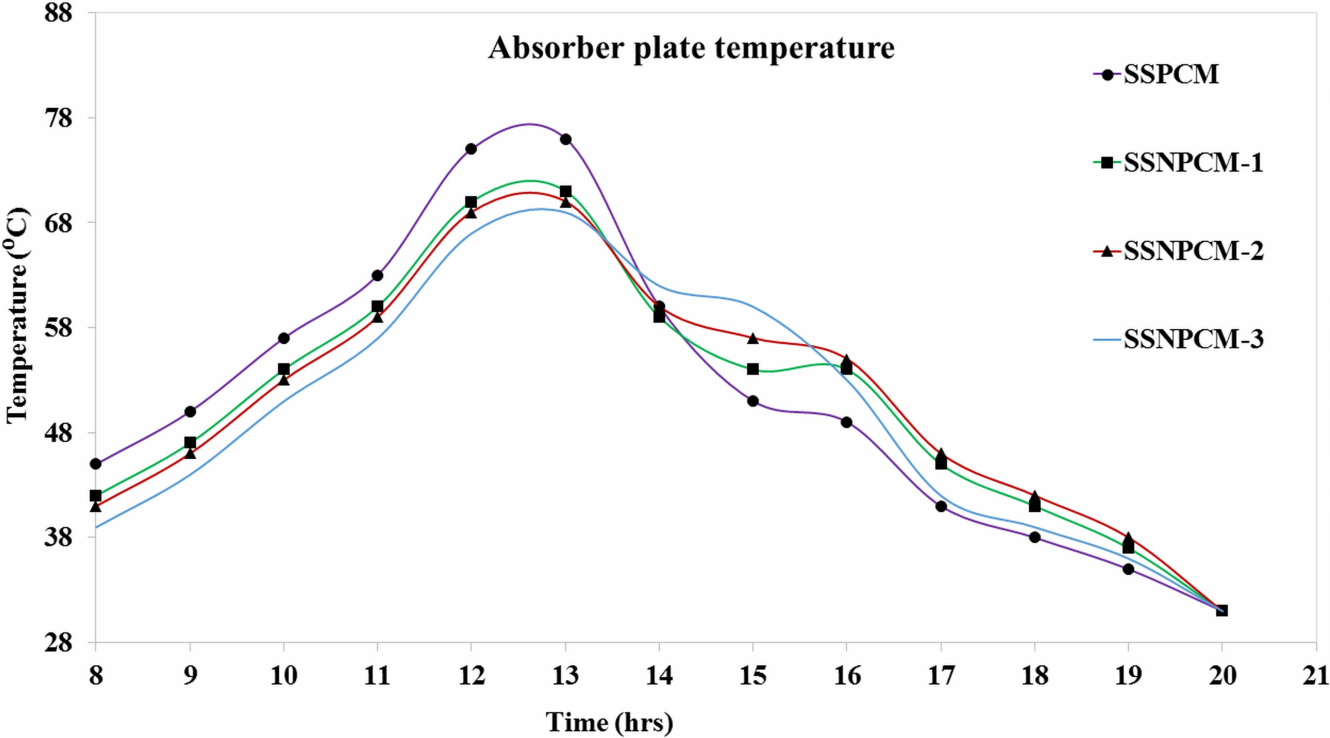
Absorber plate temperature
SSPCM
SSNPCM-1
SSNPCM-2
SSNPCM-3
Temperature (°C)
88
78
68
58
48
38
28
8
9
10
11
12
13
14
15
16
17
18
19
20
21
Time (hrs)

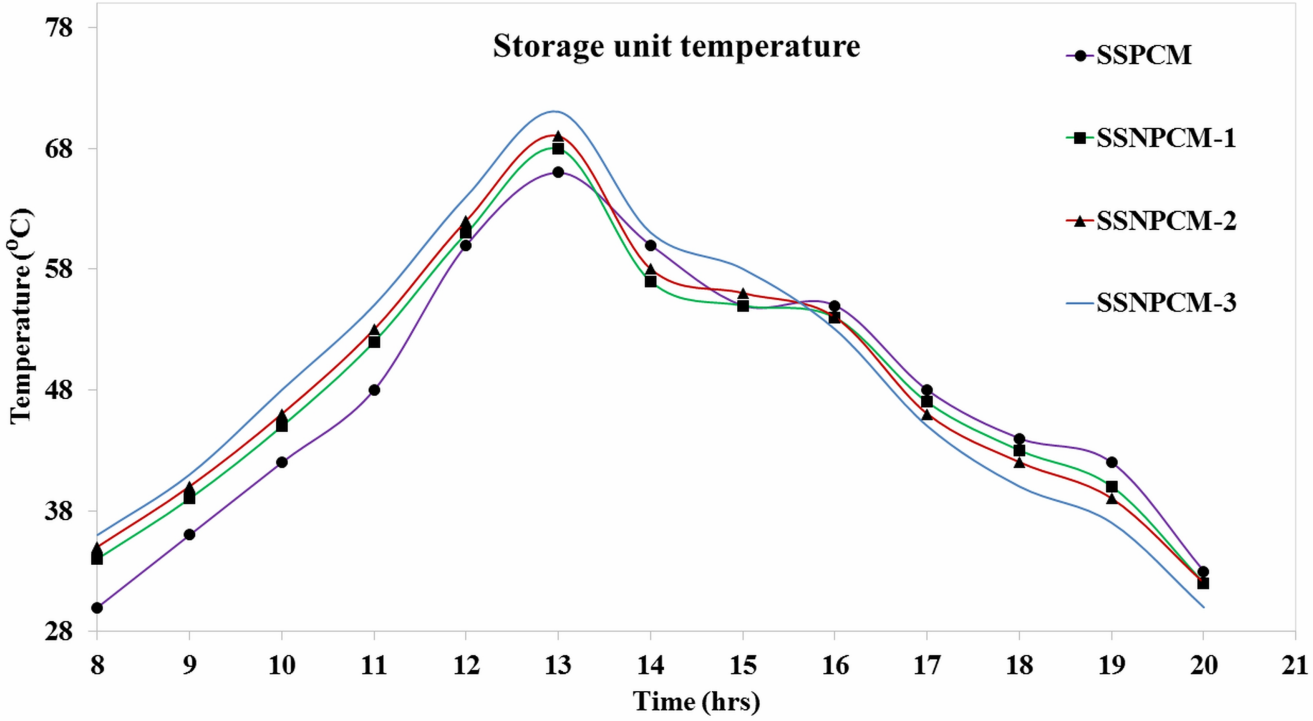
Storage unit temperature
SSPCM
SSNPCM-1
SSNPCM-2
SSNPCM-3
Temperature (°C)
78
68
58
48
38
28
8
9
10
11
12
13
14
15
16
17
18
19
20
21
Time (hrs)

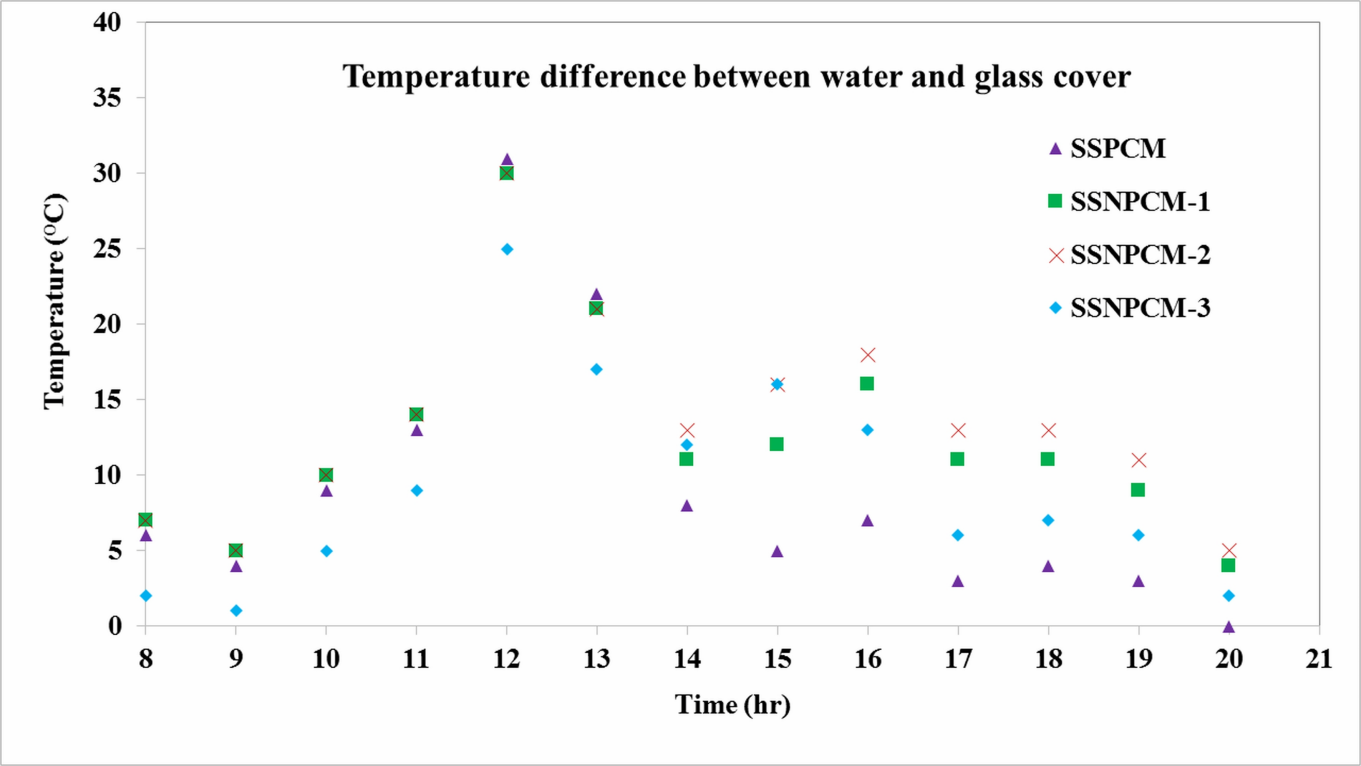
Temperature difference between water and glass cover
SSPCM
SSNPCM-1
SSNPCM-2
SSNPCM-3
Temperature (°C)
Time (hr)
0
5
10
15
20
25
30
35
40
8
9
10
11
12
13
14
15
16
17
18
19
20
21

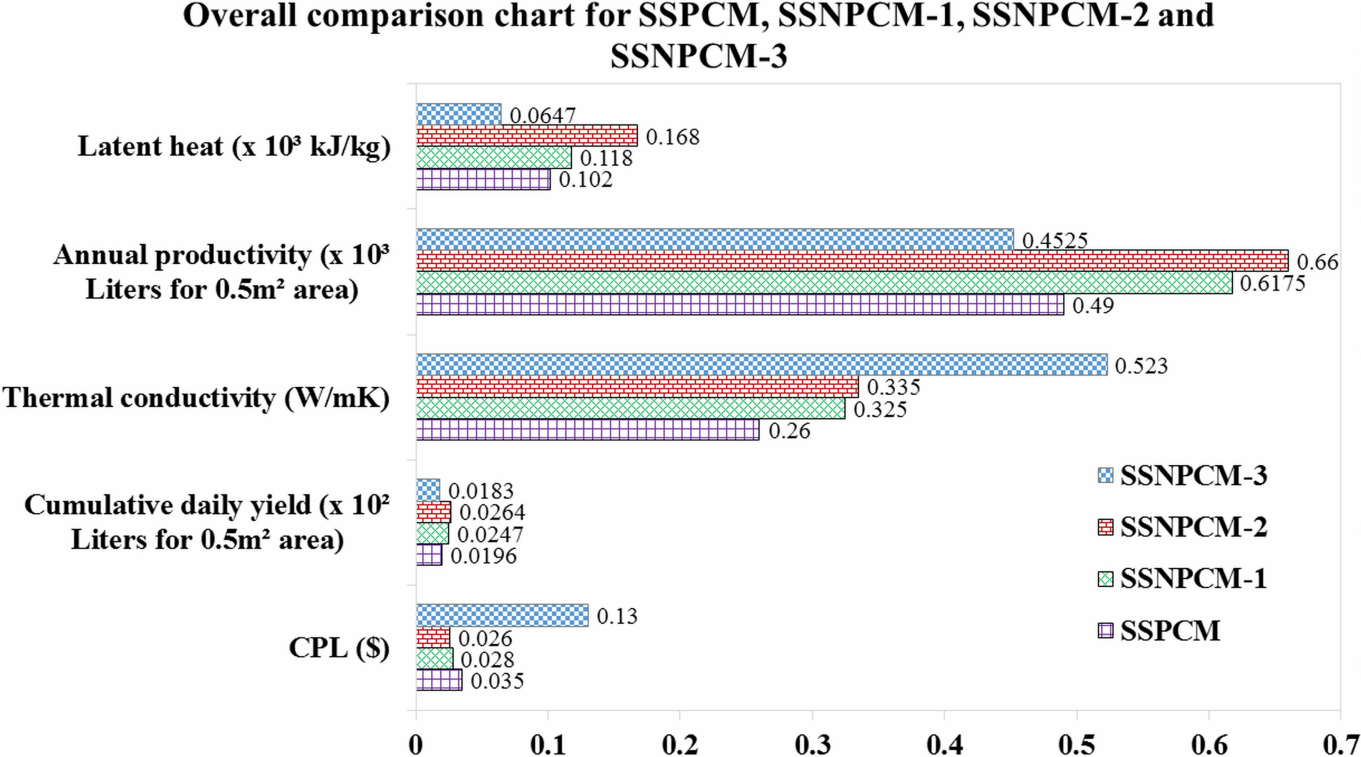
Overall comparison chart for SSPCM, SSNPCM-1, SSNPCM-2 and SSNPCM-3
Latent heat (x 10³ kJ/kg)
Annual productivity (x 10³ Liters for 0.5m² area)
Thermal conductivity (W/mK)
Cumulative daily yield (x 10² Liters for 0.5m² area)
CPL ($)
0.0647
0.168
0.118
0.102
0.4525
0.66
0.6175
0.49
0.523
0.335
0.325
0.26
0.0183
0.0264
0.0247
0.0196
0.13
0.026
0.028
0.035
SSNPCM-3
SSNPCM-2
SSNPCM-1
SSPCM
0
0.1
0.2
0.3
0.4
0.5
0.6
0.7

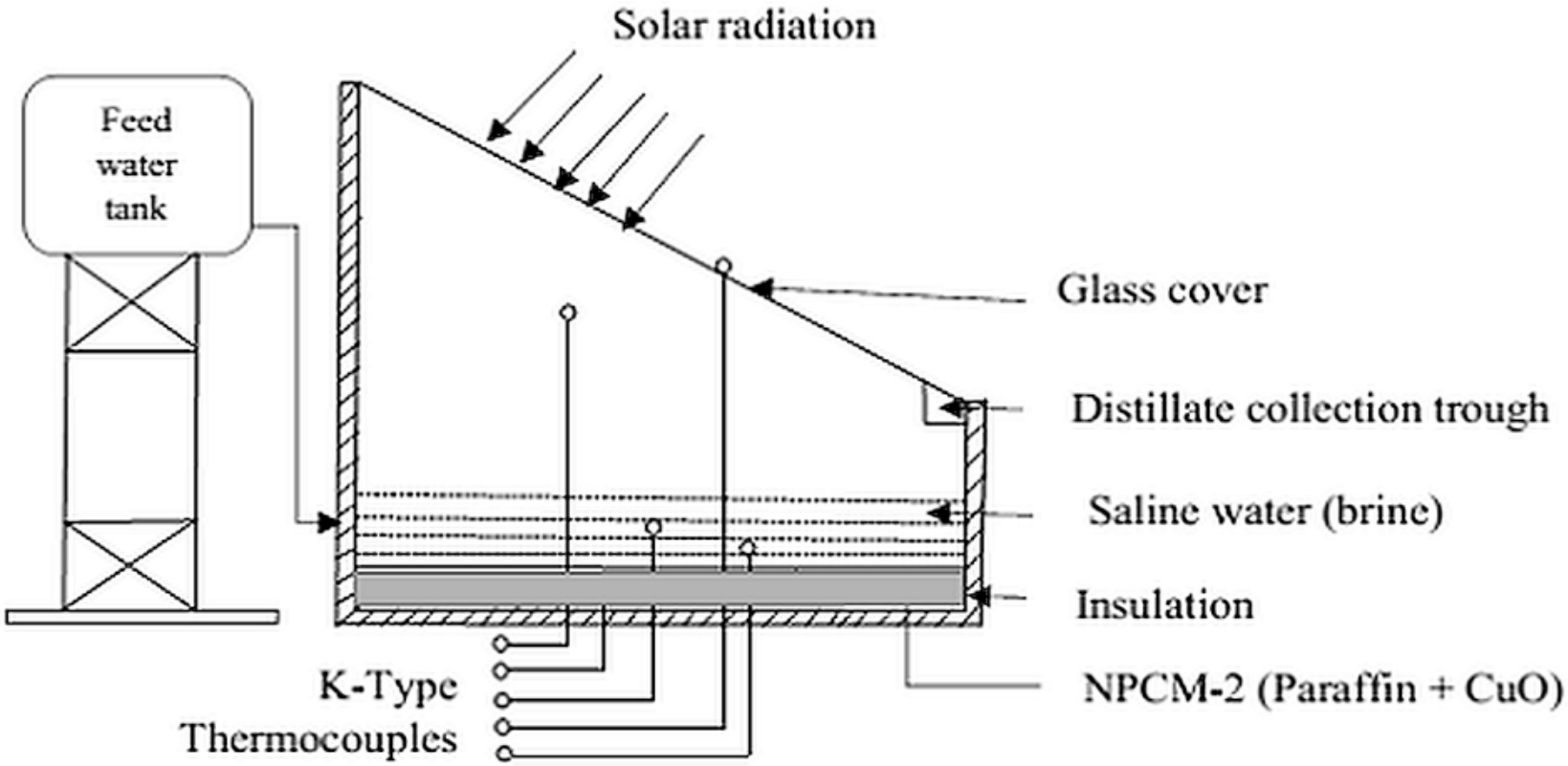

Solar still with CuO nanoparticles enhanced phase change material (NPCM-2)

Table 1

a. Overview of solar stills with sensible heat storage techniques (showing increase in yield where data are provided)

Sl. no	Authors	Material used	Location	Latitude & longitude	Productivity (L/m^2/day)	%increase in cumulative yield
1	(Sakthivel et al., 2010)	jute cloth	India	11.0168° N, 76.9558° E	4	20
2	(Kalidasa Murugavel and Srithar, 2011)	black Cotton	India	9.1674° N, 77.8767° E	3.49	
3	(Kalidasa Murugavel and Srithar, 2011)	sponge	India	9.1674° N, 77.8767° E	2.98	
4	(Kalidasa Murugavel and Srithar, 2011)	coir mate	India	9.1674° N, 77.8767° E	2.70	
5	(Kalidasa Murugavel and Srithar, 2011)	jute cloth	India	9.1674° N, 77.8767° E	3.36	
6	(Velmurugan et al., 2009, 2008a, 2008b)	sponges	India	8.7642° N, 78.1348° E	2.26	15.3
7	(Murugavel et al., 2010)	¼'' quartzite rock	India	9.1674° N, 77.8767° E	3.28	
8	(Murugavel et al., 2010)	¾''quart zite rock	India	9.1674° N, 77.8767° E	3.66	
9	(Murugavel et al., 2010)	¼'' washed stones	India	9.1674° N, 77.8767° E	3.11	

10	(Murugavel et al., 2010)	1½'' concrete pieces	India	9.1674° N, 77.8767° E	3.33	
11	(Murugavel et al., 2010)	1¼'' brick	India	9.1674° N, 77.8767° E	3.50	
12	(Murugavel et al., 2010)	mild steel	India	9.1674° N, 77.8767° E	3.30	
13	(Murugavel et al., 2010)	black cotton	India	9.1674° N, 77.8767° E	3.49	
14	(Shanmugan et al., 2012)	calcium stones	India	11.0168° N, 76.9558° E	4.28	
15	(Shanmugan et al., 2012)	white marbles	India	11.0168° N, 76.9558° E	1.89	36
16	(Manivel et al., 2014)	washed pebbles	India	11.0168° N, 76.9558° E	1.85	21
17	(Sakthivel and Shanmugasundaram, 2008)	black granite gravel	India	11.0168° N, 76.9558° E	3.9	17-20

Table 1

b. Overview of solar stills with latent heat storage techniques (showing increase in yield where data are provided)

Sl.no	Authors	Material used	Location	Latitude & longitude	Productivity (L/m^2/day)	%increase in cumulative yield
1	(El-Sebaii et al., 2009)	stearic acid	Saudi Arabia	23.8859° N, 45.0792° E	9.005	80.1
2	(Al-hamadani et al., 2014)	myristic acid	Iraq	33.2232° N, 43.6793° E	3.05	
3	(Al-hamadani et al., 2014)	lauric aicd	Iraq	33.2232° N, 43.6793° E	3.57	
4	(Swetha and Venugopal, 2011)	lauric acid	India	20.5937° N, 78.9629° E	5.1	36
5	(Shalaby et al., 2016)	paraffin	Saudi Arabia	23.8859° N, 45.0792° E	3.76	11.57
6	(Kabeel and Abdelgaied, 2016)	paraffin	Egypt	26.8206° N, 30.8025° E	7.54	67.18
7	(Asbik et al., 2016)	paraffin	Morocco	31.7917° N, 7.0926° W		80
8	(Asbik et al., 2016)	paraffin	Iran	32.4279° N, 53.6880° E	6.7	31
9	(Ansari et al., 2013)	paraffin	Morocco	31.7917° N, 7.0926° W	5.2	73
10	(Kabeel et al., 2016)	paraffin	Egypt	26.8206° N, 30.8025° E	9.36	109
11	(Mousa and Gujarathi, 2016)	paraffin	Jordan	30.5852° N, 36.2384° E	2.1	49

Table 2
Accuracy and range of the various measuring instruments used

Instrument	Make	Accuracy	Range
SEM	Carl Zeiss MA15/ EVO 18 scanning electron microscope		Resolution 3.0 nm at 30KV with SE detector Magnification : Up to 50K ~ 100K Resolution : 50 nm
TEM	CM-120-Philip transmission electron microscope		Operating voltages: 20-100 kV
DSC	Perkin Elmer-DSC 4000	±2%	Temperature range -100 to 450 ^{0}C Heating rate 5 deg/min to 20 deg/min
Anemometer	Abh-4224 - lutron electronic enterprise co., ltd.	±0.1 m/s	0.4–35 m/s
LFA	LFA 467 HyperFlash® – Light Flash Apparatus		Temperature range: -100°C to 500°C, Uncertainty < 3% Thermal conductivity : Measuring range thermal conductivity: < 0.1 W/(mK) to 2000 W/(mK) Measuring range thermal diffusivity: 0.01 mm^2/s to 1000 mm^2/s
Solarimeter	Tm-207 _ solar power meter - tenmars electronics co., ltd.	±2 W/m^2	0-3000 W/m^2
Thermocouple	Elmec heaters ltd.	±0.1 ^{0}C	0-100 ^{0}C
Beaker		±10 ml	0-1000 ml
XRD	Shimatzu diffractometer X-ray XRD 6000		Scattering angle: 20 to 80^0 Minimum step angle:0.002
TG/DTA	PerkinElmer, USA, Model Diamond TG/DTA		Operating temperature: up to 900 ^{0}C Heating rate: 20 ^{0}C/min
Thermal reliability	BIOER TC-25/H model	±0.5 ^{0}C	Temperature range: 4-99 ^{0}C
LFA	LFA 467 HyperFlash-Light Apparatus	±5%	Temperature range: -100 to 500 ^{0}C Heating rate: 50 ^{0}C/min

Table 3
Uncertainty percentage showing the values of U_i and X

Type of solar still	U_i	X_i	Uncertainty percentage (%)
SSPCM	0.0031	0.150	2.06
SSNPCM-1	0.0027	0.186	1.47
SSNCPM-2	0.0026	0.203	1.28
SSNPCM-3	0.0021	0.140	1.54

Table 4
Productivity comparison (where data are provided)

Author	Type of solar still	PCM used	Location	Productivity in '$l/m^2/day$'
(Al-hamadani et al., 2014)	Single basin single slope with PCM	Lauric acid	Iraq	3.56
(Al-hamadani et al., 2014)	Single basin single slope with PCM	Myristic acid	Iraq	3.04
(Shalaby et al., 2016)	Single basin single slope with PCM	Paraffin	Egypt	3.76
(Ansari et al., 2013)	Single basin single slope with PCM	Paraffin	Morocco	5.2
(Mousa and Gujarathi, 2016)	Single slope solar still with PCM	Paraffin	Oman	2.1
Present study	Single basin single slope with PCM	Paraffin	India	3.92
Present study	Single basin single slope with Nano-PCM	Paraffin+ Titanium dioxide	India	4.94
Present study	Single basin single slope with Nano-PCM	Paraffin+ Copper oxide	India	5.28
Present study	Single basin single slope with Nano-PCM	Paraffin+ Graphene oxide	India	3.62

Table 5
Capital cost for SSPCM, SSNPCM-1, SSNPCM-2 and SSNPCM-3

Sl. no	Materials	Present Capital Cost in US$ (for 0.5 meter square still area)			
		SSPCM	SSNPCM-1	SSNPCM-2	SSNPCM-3
1	Basin	25	25	25	25
2	Insulation	7	7	7	7
3	Stand	12	12	12	12
4	Transparent cover	8	8	8	8
5	Absorber coating	2	2	2	2
6	Fabrication cost	20	20	20	20
7	Paraffin	11.45	11.45	11.45	11.45
8	Titanium di oxide nano particles	0	0.22		
9	Graphene oxide nano particles	0	0	0	220
10	Copper oxide nano particles	0	0	0.18	0
11	other cost	4	4	4	4
12	Total cost	89.45	89.67	89.63	309.45

Table 6
Cost analysis of SSPCM, SSNPCM-1, SSNPCM-2 and SSNPCM-3

For still area= 0.5 m^2; interest per year (i)=12%, number of life years (n)=10years										
	P ($)	CRF	FAC ($)	S	SFF	ASV	AMC ($)	AC ($)	M (L/yr)	CPL ($)
SSPCM	89.45	0.177	15.83265	17.89	0.043273	0.774158	2.374898	17.43339	490	0.035578
SSNPCM-1	89.67	0.177	15.87159	17.934	0.043273	0.776062	2.380739	17.47627	617.5	0.028302
SSNPCM-2	89.63	0.177	15.86451	17.926	0.043273	0.775715	2.379677	17.46847	660	0.026467
SSNPCM-3	309.45	0.177	54.77265	61.89	0.043273	2.678179	8.215898	60.31037	452.5	0.133283

Table 7
Comparison of CPL for various solar stills with PCM

Author	PCM used	Location	Cost Per Liter (CPL) in ($)
(Shalaby et al., 2016)	Paraffin	Egypt	0.08369
(Shalaby et al., 2016)	Paraffin and wick	Egypt	0.09558
(Kabeel and Abdelgaied, 2016)	Paraffin	Egypt	0.03
Present study	Paraffin	India	0.03578
Present study	Paraffin + TiO_2 nanoparticles	India	0.028302
Present study	Paraffin + CuO nanoparticles	India	0.026467
Present study	Paraffin + GO nanoparticles	India	0.133283